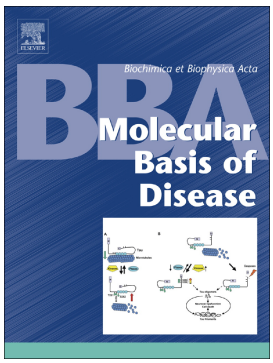

Glycogen storage in a zebrafish Pompe disease model is reduced by 3-BrPA treatment

Cinzia Bragato, Silvia Carra, Flavia Blasevich, Franco Salerno, Alessia Brix, Andrea Bassi, Monica Beltrame, Franco Cotelli, Lorenzo Maggi, Renato Mantegazza, Marina Mora

PII: S0925-4439(20)30001-6

DOI: https://doi.org/10.1016/j.bbadis.2020.165662

Reference: BBADIS 165662

To appear in: *BBA - Molecular Basis of Disease*

Received date: 23 October 2019

Revised date: 16 December 2019

Accepted date: 2 January 2020

Please cite this article as: C. Bragato, S. Carra, F. Blasevich, et al., Glycogen storage in a zebrafish Pompe disease model is reduced by 3-BrPA treatment, *BBA - Molecular Basis of Disease*(2020), https://doi.org/10.1016/j.bbadis.2020.165662

Glycogen storage in a zebrafish Pompe disease model is reduced by 3-BrPA treatment.

[1,2]**Cinzia Bragato, [3]Silvia Carra, [2]Flavia Blasevich, [2]Franco Salerno, [2]Alessia Brix, [4]Andrea Bassi, [5]Monica Beltrame, [5]Franco Cotelli, [2]Lorenzo Maggi, [2]Renato Mantegazza and [2]*Marina Mora.

[1]PhD program in Neuroscience, University of Milano-Bicocca, Via Cadore 48, Monza, 20900, Italy.
[2]Neuromuscular Diseases and Neuroimmunology Unit, Fondazione IRCCS Istituto Neurologico Carlo Besta, Via Celoria 11, Milan, 20133, Italy.
[3]Laboratory of Endocrine and Metabolic Research, IRCCS Istituto Auxologico Italiano, Piazzale Brescia 20, Milan, 20149, Italy.
[4]Department of Physics, Politecnico di Milano, Piazza Leonardo da Vinci 32, Milan, 20133, Italy.
[5]Department of Biosciences, Università degli Studi di Milano, Via Celoria 26, Milan, 20133, Italy.

Running title: **Zebrafish model of Pompe disease**

*Corresponding author:
Marina Mora, marina.mora@istituto-besta.it

**Co-corresponding author:
Cinzia Bragato, cinzia.bragato@istituto-besta.it

Muscle Cell Biology Lab,
Fondazione IRCCS Istituto Neurologico Carlo Besta
Via Temolo 4, 20126 Milano, Italy
Tel. +39-022394632; Fax: +39-022394619;

ABSTRACT

Pompe disease (PD) is an autosomal recessive muscular disorder caused by deficiency of the glycogen hydrolytic enzyme acid α-glucosidase (GAA). The enzyme replacement therapy, currently the only available therapy for PD patients, is efficacious in improving cardiomyopathy in the infantile form, but not equally effective in the late onset cases with involvement of skeletal muscle. Correction of the skeletal muscle phenotype has indeed been challenging, probably due to concomitant dysfunctional autophagy. The increasing attention to the pathogenic mechanisms of PD and the search of new therapeutic strategies prompted us to generate and characterize a novel transient PD model, using zebrafish. Our model presented increased glycogen content, markedly altered motor behavior and increased lysosome content, in addition to altered expression of the autophagy-related transcripts and proteins Beclin1, p62 and Lc3b. Furthermore, the model was used to assess the beneficial effects of 3-bromopyruvic acid (3-BrPA). Treatment with 3-BrPA induced amelioration of the model phenotypes regarding glycogen storage, motility behavior and autophagy-related transcripts and proteins. Our zebrafish PD model recapitulates most of the defects observed in human patients, proving to be a powerful translational model. Moreover, 3-BrPA unveiled to be a promising compound for treatment of conditions with glycogen accumulation.

Keywords: Pompe disease, acid α-glucosidase, zebrafish, glycogen, 3-Bromopyruvic acid (3-BrPA).

Abbreviations: 3-Bromopyruvic acid (3-BrPA), Hexokinase (HK), 2-(N-(7-nitrobenz-2-oxa1,3-diazol-4-yl)-amino)-2-deoxyglucose (2-NBDG), morpholino (MO), standard control morpholino (STD-Ctrl), hours post fertilization (hpf), days post fertilization (dpf).

INTRODUCTION

Pompe disease (PD), also called glycogenosis type II, is an autosomal recessive metabolic disorder due to a defect in the lysosomal enzyme acid α-glucosidase (GAA), or acid maltase, necessary for glycogen degradation. The defect results in generalized excessive glycogen accumulation in tissues, involving in particular skeletal and cardiac muscle.

The spectrum of disease severity encompasses a broad continuum of phenotypes ranging from the most severe “classic” form, characterized by child onset, severe cardiomyopathy, rapidly progressive course and fatal outcome before two years of age, to the “intermediate” infantile form with milder phenotype, to the juvenile and adult forms with prevalent involvement of skeletal muscle [1]. The almost total deficiency of the enzyme results in the severe infantile form, while partial deficiency is responsible for the intermediate and mild forms [2-3]. The enzyme replacement therapy (ERT), the only medication available since 2006, has represented a major step in the treatment of patients with Pompe disease and, although gene therapy is in clinical trial, currently it remains the only FDA-approved therapy. ERT has shown to be effective in improving cardiomyopathy in the infantile severe Pompe disease form; however, despite clinical benefits for most patients [4-8] the late onset cases do not all respond equally well to treatment, and a number of reports suggests that correction of the skeletal muscle phenotype is particularly challenging, probably due to concomitant altered autophagy [9-12]. However, it remains unclear how autophagy, a key molecular mechanism that maintains cellular homeostasis and ensures correct macromolecule turnover in the cell [13-15], is responsible for GAA failure to restore muscle function, since it is yet unknown if an excessive acceleration or reduction of the process is present in Pompe disease.

The possible role of altered autophagy has stimulated both reassessment of the pathogenic mechanisms and investigation of novel therapeutic approaches in Pompe disease, including searching for adjunctive and alternative therapies addressing both glycogen accumulation and autophagy [16-21].

Among the small molecules to be explored for interfering with glycogen accumulation, we have developed an interest on 3-bromopyruvate (3-BrPA), an inhibitor of hexokinase (HK), which is a key glycolytic enzyme. *In vitro* and *in vivo* studies have reported that 3-BrPA is an anti-tumor drug effective in those tumor phenotypes in which cancer cells preferentially depend on glycolysis to produce adenosine triphosphate (ATP) for growth and proliferation

[22-25]. This phenotype, referred to as 'aerobic glycolysis', was first observed by Warburg in 1924. The anti-cancer property of 3-BrPA is due to its ability to inhibit glycolysis, by abolishing cell ATP production and, consequently, preventing the hexokinase transformation of glucose into glucose-6-phosphate [26], and to trigger activation of the autophagic process [27].

In mammals, separate genes code for different hexokinase isoforms: HKI, HKII, HKIII, and HKIV. HKII is expressed at relatively high levels only in skeletal muscle, adipose tissue, and heart. HKII is responsible for the conversion of glucose to glucose-6-phosphate in the first step of glycolysis without being regulated by negative feedback (product inhibition) as are the other hexokinase isoforms [28]. Furthermore, HKII is reported to be one of 3-BrPA's major targets [29,30] among all the other hexokinase isoforms.

3-BrPA, having structural similarity with lactate, is likely to be transported across the plasma membrane of cells by the proton-linked monocarboxylate transporter (MCTs) [31]. Of the 9 known MCT-related sequences in mammals, MCT1 is ubiquitously expressed, but is especially prominent in heart and red muscle [32].

At present, the best characterized animal model of PD is the GAA-knockout murine model which lacks *Gaa* mRNA transcription and displays a virtually complete acid α-glucosidase deficiency [33]. Such a model does not recapitulate the genetics of patients affected by late onset Pompe disease, in whom hypomorphic GAA mutations are present [34].

In the present study, we generated a novel transient PD model, taking advantage of zebrafish, to better recapitulate the pathophysiology of these PD patients.

Zebrafish, as reported in the literature in the past years, is a suitable model to study autophagy [35,36]. Moreover, zebrafish hexokinases isoforms and their proton-linked monocarboxylate transporters are very similar and comparable to the mammalian ones [37,38], making zebrafish a reliable model for studying 3-BrPA effects.

In the present study, we characterized the PD zebrafish transient model using two different morpholinos (a translation-blocking morpholino, against the start codon ATG and a splice-blocking morpholino, against a specific portion between intron 9 and exon 10 of the zebrafish gaa gene). We investigated the effects of rescuing the resulting phenotypes of the latter by injecting an *in vitro* transcribed *gaa* RNA. In gaa morphants we assessed skeletal muscle condition at optical and electron microscopy level, determined glycogen accumulation, and evaluated motor behaviour by touch evoked motility test. Finally, we assessed possible beneficial effects of 3-BrPA treatment on glycogen storage, on autophagy related transcripts and proteins and on motility behaviour.

MATERIALS AND METHODS

Animal care

Fish were raised and maintained according to good animal practice principles as defined by the Italian animal welfare regulations. All experiments were performed on embryos and larvae within 5 days post fertilization (dpf), thus not subject to animal experimentation rules according to European and Italian directives.

RNA extraction and reverse transcription

Total RNA was extracted from zebrafish embryos at different stages, from 1 cell stage to 5 dpf, using TRI Reagent (MRC, Cincinnati, OH, USA). First-strand cDNA synthesis reaction from total RNA was catalyzed by Transcriptor First Strand cDNA Synthesis Kit (Roche Diagnostic, Penzberg, Germany). cDNA was amplified with specific primers using Phusion High-Fidelity polymerase (Finnzymes, Thermo Fisher Scientific, Waltham, MA, USA). The PCR products were purified using Illustra ExoProStar (GE Healthcare, Life Sciences, WI, USA) and sequenced directly with BigDye Terminator v1.1 Cycle Sequencing Kit (Applied Biosystems, Life Technologies, Carlsbad, CA, USA). Sequences were analyzed on an ABI Prism 3100 Genetic Analyzer (Applied Biosystems, Life Technologies, Carlsbad, CA, USA). The primers used to clone the cDNA in the vector were: *gaa*: 5′-ACATCACAGGAAAATGGCGG -3′ (Forward) and 5′-TCCCGTGAACTTGTAACAGC -3′ (Reverse). Primers used to visualize I9E10*gaa*-MO in-frame intron retention were: 5’-CTTTACTTTCGACCCGCAGC -3’(Forward) and 5’- AACGGCCGAGTTTTCTTCAC -3’ (Reverse).

Morpholino injections

Zebrafish *gaa* was knocked down with two different antisense morpholinos: one, called ATG*gaa*-MO, directed against the translation start site of the *gaa* transcript, 5′-CTTCATGTATTAAACACAGGGCTGT-3′, and one, called I9E10*gaa*-MO, targeting the splice site between intron 9 and exon 10, close to the region encoding the catalytic site of the Gaa protein, 5′-tgtgattttcttgtttacagGACAT-3′. The latter, in particular, causes retention of intron 10, resulting in insertion of 14 aberrant amino acids and in premature stop codon. Both morpholinos were designed and purchased, along with a standard control morpholino (STD-Ctrl), from Gene Tools (Gene Tools, Philomath, OR, USA).

Fertilized eggs, collected after timed mating of adult zebrafish, were injected at the 1-2 cell stage using an Eppendorf transferman nk2 micromanipulator (Eppendorf AG, Hamburg, Germany). Embryos were injected with either ATG*gaa*-MO (0.8 pmol/embryo), or I9E10*gaa*-MO (1 pmol/embryo), or STD-Ctrl (to verify absence of morpholino-mediated toxicity), diluted in Danieau solution in a volume of 4 nl [39]. To monitor the injection either rhodamine dextran (Molecular Probes, Life Technologies, Carlsbad, CA, USA) or phenol red (Sigma Aldrich, Saint Louis, MO, USA) were co-injected as tracers and observed under a Leica MZ FLIII microscope (Leica Microsystems GmbH, Wetzlar, Germany).

For rescue experiments, embryos were injected (4 nl total volume) with I9E10*gaa*-MO plus *gaa* mRNA (10pg). After injection embryos were allowed to develop in fish water at 28 °C up to the stage of interest.

Phenotypic assessment was conducted by visual assessment using a stereomicroscope Leica MZ FLIII. Embryo phenotypes were subdivided based on the morphological features described in Kimmel et al., 1995 [40]. Deformities included abnormally curled tails, shortened body length, abnormal somite structure, etc.

Western Blot

Dechorionated embryos (minimum 10 per experiment) were boiled for 10 min at 95^{o}C. Twenty µg of protein samples were electrophoresed on 10% SDS-PAGE and transferred to nitrocellulose membranes (Bio-Rad Laboratories, Hercules, CA, USA) following standard procedures. The amount of loading proteins was previously determined with serial dilutions (10, 20, 50 µg) in order to have bands of adequate intensity to be detected within the linear range. α-Tubulin, used as loading control, was also diluted in the linear range. The membranes were blocked with 5% nonfat dry milk in TBS, pH 7.5, containing 0.1% Tween 20 (TBST) for 1 h at room temperature, incubated with antibodies reported in Table 2.

Yolk removal

For sedation Dechorionated embryos were placed, using a plastic pipette, in an eppendorf tube (1.5 ml) on ice, for sedation. The embryos were then placed at room temperature (RT), as much fluid (fish water/egg water) as possible was removed from the tube, and deyolking buffer (1/2 Ginzburg fish Ringer solution) was added (*). The yolks were gently removed with a 200 µl pipette tip. The embryos were let floating down to the bottom of the

tube, and as much deyolking fluid as possible was removed, 2 rinses with ice cold Ringer's solution followed with liquid removal each time.

(*) Deyolking buffer**:**

To obtain 400 ml of deyolking buffer, 0.04 g of $NaHCO_3$ were added to a solution composed of 1.3 g NaCl, 0.05 g KCl, 0.06 g $CaCl_2$ or 0.08 g $CaCl_2$ $2H_2O$ in 350 ml milliQ water, and adjusted to a final volume of 400 ml with further milliQ water. The solution was filtered and stored at RT.

Glycogen Assay

The glycogen amount was determined in dechorionated zebrafish embryos (minimum 10 per experiment), after yolk removal, by the Glycogen Assay kit II (Abcam, Cambridge, England) according to the manufacturer's instructions.

Embryo morphological characterization

Zebrafish at 4 dpf were fixed 2 h in 2.5% glutaraldehyde-sodium phosphate buffer, pH 7.4; left in buffer overnight at 4 °C; post-fixed 1 h in 2% phosphate-buffered OsO4, dehydrated in graded ethanol, and embedded in epoxy resins (Electron Microscopy Sciences, Hatfield, Pennsylvania). Semi-thin sections (1 µm thick) were examined by light microscopy after toluidine blue staining. Ultrathin sections of zebrafish tails were collected onto grids, stained with uranyl-less (Electron Microscopy Sciences) and Reinold's solution, and examined with a FEI Tecnai G2 Spirit electron microscope (FEI Hillsboro, Oregon, United States).

Periodic acid–Schiff (PAS) staining

Resin was removed with sodium methoxide (3') from semi-thin sections of 4 dpf zebrafish, followed by methanol (5') and ethanol (5'). For staining, sections were placed in: Carnoy fixative (15'); 2% periodic acid (15'); and Schiff reactive (1 hour in the dark); then they were dehydrated and mounted.

LysoTracker Red dye staining

LysoTracker Red (Thermo Fisher Scientific) was added to embryos at 24 hours post fertilization (hpf) in 48-well plates, at a final concentration of 10 µM. The embryos were incubated at 28.5°C for 45 minutes. Then, the water was removed and the embryos were

rinsed three times with approximately 1 ml fresh fish water immediately before fluorescence microscopy imaging, as described [41].

Glycogen visualization with 2-NBDG

2-(N-(7-nitrobenz-2-oxa1,3-diazol-4-yl)-amino)-2-deoxyglucose (2-NBDG) was used to verify if glycogen could be visualized *in vivo*. This is a fluorescent synthetic glucose analog, hypothetically suitable to be incorporated within the multi-branched polysaccharide glycogen chain rendering it fluorescent. Two hundred pg/embryo of 2-NBDG were injected into wild type embryos at 1 cell stage. Embryos were examined under an epifluorescence microscope at somitogenesis stage and at 24 hpf, and fluorescent glycogen accumulation could be detected in the somites and in the tail (Supplementary Figure 1). The limitation of this experiment is that 2-NBDG fluorescent signal is visible for about 24 hours, therefore only in embryos until 1 dpf. A different approach is thus required to detect glycogen in later developmental stages.

Quantification

To quantify the LysoTracker dye, tricaine treated embryos were observed under an epifluorescence microscope and pictures of the entire tail, starting from one somite before the end of the yolk, were taken at 10X. The red signal area (expressed as arbitrary units) was calculated by means of Fiji software (https://imagej.net/Fiji) on images taken at same exposure conditions [42]. Using the software, a threshold was applied to the pictures to obtain red and black images with regions positive for LysoTracker in red and negative in black. The area positive for LysoTracker was calculated as a percentage of the entire image, and the mean percentage area was then obtained. The same procedure as before was used to quantify the 2-NBDG green signal.

The quantitation of the western blot bands was performed on membranes from three different experiments using Fiji software. To perform the analysis, for each protein and loading control, a region of interest (ROI) was defined and saved. The same ROI was applied to the other two membranes images, in order to take measurements in the same way for the bands and their background. The ratios between protein band of interest and loading control band, expressed as arbitrary units, were then exported into an excel file and analyzed using Graph-pad Prism software.

qRT-PCR

Transcripts of wild-type *gaa* and of genes related to autophagy were evaluated by qRT-PCR using primers reported in Table 1. PowerUp SYBR Green Mastermix (Thermofisher) and ABI Prism 7000 (Applied Biosystem) PCR systems were used for quantification. ΔΔCt method was used to calculate the relative copies of mRNAs of the gene of interest, normalized to the reference gene mRNA (Table 1).

gaa mRNA injection

The cDNA of full-length zebrafish *gaa* was amplified by RT-PCR using total RNA extracted from whole zebrafish embryos. The primer sequences used were 5′-GCAGGATCCCATCGATGGACATCACAGGAAAATGGCGG -3′ (sense primer plus ClaI sequence) and 5′- GTTCTAGAGGCTCGAGCCTCCCGTGAACTTGTAACAGC -3′ (antisense primer plus XhoI sequence) for zebrafish *gaa* cDNA. The amplified fragments were inserted into pcGlobin2 vector [43]. After digestion of pcGlobin2 vector with appropriate restriction enzymes (ClaI and XbaI, New England biolabs, Ipswich, MA; and XhoI; Promega Corporation, Madison, WI, USA), the amplified cDNA of *gaa* was cloned into pcGlobin2 vector to obtain the pcGlobin2-*gaa* construct.

Plasmids were linearized with XbaI enzyme (New England Biolabs, Ipswich, MA, USA) and transcribed using the T7 mMessage Machine kit (Ambion, Life Technologies, Carlsbad, CA, USA). Fertilized eggs were injected at the one to two cell stage with zebrafish *gaa* mRNA (10 pg), in a 4 nl volume, using a microinjector (Leica).

3-BrPA treatment

Different concentrations of 3-BrPA, starting from 20 μM to 2 mM, diluted in 20 ml of fish water, were tested, based on published data [44], to evaluate the dose-dependent mortality range (Supplementary Figure 2). A concentration of 100 μM was chosen to treat the embryos at 60% epiboly stage. Since the 3-BrPA molecule dimension is such that it can cross the chorion barrier, the treatment was administered to embryos with chorion.

Screening for embryonic motility

Larvae were subjected to a tactile stimulus at 3 dpf: using a needle, a gentle stimulus was applied to the tail of the zebrafish larvae and their reaction observed (touch-evoked motility test) [45]. Upon application of the tactile stimulus wild type larvae at this stage of development normally swim away from the source of the stimulus, while embryos injected

with morpholino oligonucleotides to knock down genes related to motility show variably reduced motility.

Data Analysis

In all knock down experiments, ATG*gaa*- and I9E10*gaa*-MO-injected embryos were compared to embryos at the same developmental stage, injected with the same amount of a control standard morpholino.

Results were expressed as means ± standard deviation. Differences between groups of morphants in basal conditions (ATG*gaa*-MO or I9E10*gaa*-MO vs STD-Ctrl, 3-BrPA-treated or non-treated) and differences between groups in rescue experiments (I9E10*gaa*-MO, treated and non-treated, and STD-Ctrl) were assessed by the two-tailed Student T test. P values were considered significant: *$p \leq 0.05$, **$p \leq 0.01$; ***$p \leq 0.001$. For graphs, Graph-pad Prism software was used; for figures, Adobe Photoshop was used.

RESULTS

Characterization of the model

Zebrafish *gaa* gene

The *gaa* zebrafish transcript (variant X1) corresponding to NCBI XM_001921922.5 was identified. This is the only full length coding sequence present in zebrafish, located on chromosome 3, and reported as the orthologous of the human gene acid alpha glucosidase (GAA). The identity between the human GAA and the zebrafish Gaa protein is 58% (from Genomicus, www.genomicus.biologie.ens.fr/genomicus/cgi-bin/search.pl). This good similarity is due to the conservation of all the functional domains (Trefoil domain, GH31_N Domain, GH31_MGAM_SI_GAA Domain and Glyco_Hydro_31 Domain) of the protein.

The characterization of *gaa* expression, performed by qRT-PCR, showed that the *gaa* transcript is present from the first stages of development up to 5 days post fertilization (Supplementary Figure 3).

gaa knocked-down embryos displayed phenotypic defects and increased glycogen content

Both *gaa* morpholinos were tested at a range of concentrations (from 0.5 pmol/embryo to 1.5 pmol/embryo) and dose-dependent phenotypic classes were observed. Based on the observed phenotypic classes, in order to obtain embryos with glycogen accumulation in skeletal muscle, but with an overall conserved somite structure, ATG*gaa*-MO was injected at a concentration of 0.8 pmol/embryo and I9E10*gaa*-MO at a concentration of 1 pmol/embryo. Since I9E10*gaa*-MO injected embryos showed a slight growth delay at early stages of development, the phenotypes were examined at 3 dpf.

ATG*gaa*-MO injection resulted in reduced Gaa protein amount, as evaluated by western blot, (Supplementary Figure 4A), and injection of I9E10*gaa*-MO causing an out-of-frame insertion due to activation of a cryptic splice site (see https://www.gene-tools.com/choosing_the_optimal_target#blockingnuclearprocessing), resulted in a higher aberrant transcript band, as evaluated by RT-PCR, and in lack of the aberrant protein band by western blot (Supplementary Figure 4B).

At the chosen concentrations, of the embryos injected with ATG*gaa*-MO, 285 (69 % of total) pertained to the C1 class with normal-appearing morphology and completely formed somites, 95 (23% of total) pertained to the C2 class with partially disrupted somites, and 36 (8% of total) pertained to the C3 class (Supplementary Figure 5) with unformed or totally disrupted somites; whereas, of the embryos injected with I9E10*gaa*-MO, 225 (53% of total) were belonging to the C1 class, 121 (29% of total) to the C2 class, and 74 (18% of total) embryos to the C3 class (Figure 1A, B). Of note, in the I9E10*gaa*-MO morphants belonging to the C2 class (121 embryos in total), features such as cardiac edema (in 56 morphants), enlargement of the IV cerebral ventricle (in 45 morphants) or both alterations (in 20 morphants) were observed (Figure 1A).

In order to evaluate if knock-down of the *gaa* was recapitulating the human glycogen storage condition in skeletal muscle, glycogen amount was measured in ATG*gaa*-MO and I9E10*gaa*-MO morphants belonging to the C1 class using a commercial glycogen assay kit. A significant glycogen increase was observed in ATG*gaa* morphants (ATG*gaa*-MO: 72.25 ± 0.323 vs STD-Ctrl: 43.00 ± 0.204; $p<0.0001$), compared to control embryos, which was even greater in I9E10*gaa* morphants (I9E10*gaa*-MO: 122.5 ± 0.540 vs STD-Ctrl: 43.00 ± 0.204; $p<0.0001$) (Figure 1C).

In summary injection of both ATG*gaa*-MO and I9E10*gaa*-MO morpholinos caused defects in the embryo morphology and an increase in glycogen content, more marked in the latter.

Morphological features were altered in muscle and heart of *gaa* knocked down embryos

Toluidine blue-stained transverse and longitudinal semithin sections of ATG*gaa* and I9E10*gaa* morphants, at 4 dpf, showed increased space surrounding muscle fibres, often occupied by blue violet material, not observed in STD-Ctrl embryos (Figure 1D, upper panel). Such blue violet material corresponds to glycogen, which, by Periodic acid–Schiff (PAS) reaction stains fuchsia (Figure 1D, lower panel). At electron microscopy level, increase in glycogen particles, and presence of lysosomal-related elements, such as vesicles, electron dense bodies, and small membranous corpuscles, were observed around muscle fibres in both ATG*gaa* and I9E10*gaa* morphants, more evident in the latter (Figure 1E).

Furthermore, the heart of 4 dpf morphants and control embryos, analyzed at morphological level showed increase of blue violet material in pericardial muscles and increase of pericardial fluid in I9E10*gaa* morphants, compared to controls (Figure 1F). Moreover, morphant's heart revealed laxity of the ventricle and augment of the cardiac jelly layer (Figure 1F, b''), compared to the control embryo heart.

In summary, in both morphants glycogen appeared increased by PAS and toluidine blue staining; glycogen particle increase and lysosomal-related elements were observed by electron microscopy; and morphological defects were found in the heart.

Motility was defective in *gaa* knocked down embryos

The touch evoked response test was performed on ATG*gaa* and I9E10*gaa* morphants belonging to the C1 class at 3 dpf. In comparison to STD-Ctrl-injected embryos, a slight escape attempt was present in 21 ATG*gaa* morphants out of 30, with evident muscle stiffness. Motility defects were more severe in I9E10*gaa* morphants: 26 injected embryos out of 30 showed very weak escape contraction, and obvious muscle stiffness (Supplementary Videos 1 and 2).

Lysosomal content was more increased in ATG*gaa* than in I9E10*gaa* morphants

To track lysosomes in vivo, LysoTracker dye was added to ATG*gaa*-MO-, I9E10*gaa*-MO- and STD-Ctrl-MO-injected embryos at 24 hpf. All embryos had been previously injected with 2-NBDG at one cell stage. 2-NBDG, a D-glucose fluorescent derivative used to monitor glucose incorporation into glycogen [46], was used to label glycogen *in vivo*.

Quantitation of the LysoTracker red signal showed that ATG*gaa* morphants had a significant red signal increment compared to STD-Ctrl (ATG*gaa*-MO: 12360 ± 3195 vs STD-Ctrl: 5154 ± 885.8; p=0.0289), while I9E10*gaa* morphants displayed a red signal comparable to STD-Ctrl (I9E10*gaa*-MO*:* 6070 ± 837.0 vs STD-Ctrl: 5154 ± 885.8; p=0.4588) (Figure 1G).

Quantitation of the 2-NBDG green signal showed a significant increase in the green dot area in both *gaa* morphants, compared to STD-Ctrl (ATG*gaa*-MO: 5261 ± 702.7 vs STD-Ctrl: 3300 ± 377.0; p= 0.0200; I9E10*gaa*-MO*:* 6077 ± 851.9 vs STD-Ctrl: 3300 ± 377.0; p=0.0023) (Figure 1H).

Tracking *in vivo* of lysosomes and glycogen by fluorescent dyes showed increase in lysosomes only in ATG*gaa* morphants, while glycogen was increased in both.

Expression of autophagy-related transcripts and proteins was altered in I9E10*gaa* morphants

At 48 hpf, *atg7, atg4, beclin1, mtor, p62, lc3b* and *ulk1* transcript levels by qRT-PCR were not significantly different in ATG*gaa* morphants compared to STD-Ctrl embryos (not shown). In I9E10*gaa* morphants a significant increase in *lc3b* (I9E10*gaa*-MO: 2.284 ± 0.297 vs STD-Ctrl: 0.9998 ± 0.225; p=0.0138) and *beclin1* transcript levels (I9E10*gaa*-MO: 2.259 ± 0.301 vs STD-Ctrl: 1.015 ± 0.102; p=0.0078) was observed, compared to STD-Ctrl (Figure 2A).

Proteins related to autophagy Lc3, p62, mTOR, p-mTOR, AMPk, p-AMPk, Lamp2 and Beclin1, quantitated on Western blot bands, at 24 hpf, were not significantly different in both morphants compared to STD-Ctrl embryos (Supplementary Figure 6); whereas, in I9E10*gaa* morphants, at 4 dpf, p62 (I9E10*gaa*-MO: 1.037 ± 0.2109 vs STD-Ctrl: 0.2733 ± 0.05925; p=0.0252) and Lc3b (measured as ratio Lc3bII/Lc3bI) (I9E10*gaa*-MO: 1.790 ± 0.01155 vs STD-Ctrl: 0.8600 ± 0.05568; p<0.0001) were significantly increased compared to STD-Ctrl (Figure 2B).

In summary, among autophagy-related transcripts and proteins, *lc3b* and *beclin1* mRNA levels were significantly increased at 48hpf, and p62 and Lc3b proteins were significantly increased at 4dpf in I9E10*gaa*, but not in ATG*gaa* morphants.

***gaa* mRNA injection rescued Pompe disease phenotype in I9E10*gaa* morphants**

To avoid base-pairing between the oligomer and the in vitro synthetized mRNA that could occur with ATG*gaa* morpholinos, the rescue experiment was performed exclusively in

I9E10*gaa* morphants (hereinafter called rescued I9E10*gaa* morphants). One-cell stage embryos were co-injected with I9E10*gaa*-MO (1 pmol/embryo) and 10pg/4nL *gaa* mRNA. The resulting phenotypes were compared with I9E10*gaa* morphants and with STD-Ctrl embryos and the distribution of the phenotypes, based on the correct formation of somites, was annotated at 24 hpf (Figure 3A). To classify the phenotypes, correct morphology (Figure 3Ba), developmental delay (Figure 3Bc) and deformities (Figure 3Be) were considered. The rescued morphants presented a significant increase in the number of embryos with correct morphology, compared to non-rescued I9E10*gaa*-MO (I9E10*gaa*-MO + *gaa* mRNA: 14.80 ± 1.158 vs I9E10*gaa*-MO: 6.200 ± 0.8602; p=0.0003). No significant differences were observed in growth retardation between rescued and non-rescued I9E10*gaa* morphants; while deformities were significantly less in rescued I9E10*gaa* morphants compared to non-rescued (I9E10*gaa*-MO + *gaa* mRNA: 5.0 ± 0.3162 vs I9E10*gaa*-MO: 12.60 ± 2.379; p=0.0133) (Figure 3B, C).

The embryos were then let develop in fresh fish water and again observed at 48 hpf. At this developmental stage, although the I9E10*gaa* morphants presented fewer morphological defects, rescued morphants still showed significantly higher numbers of embryos presenting an appropriate body and somite formation (Figure 3Bb) (I9E10*gaa*-MO + *gaa* mRNA: 18.20 ± 2.672 vs I9E10*gaa*-MO: 10.40 ± 1.860; p=0.0435). Numbers of morphants with growth retardation (Figure 3Bd) or deformities (Figure 3Bf) were not significantly different between rescued and non-rescued morphants at this developmental stage. Rescued morphants presenting cardiac edema, enlargement of the IV cerebral ventricle or both, were fewer than non-rescued morphants, but, again, the difference was not significant.

Rescue with gaa mRNA on glycogen storage was assessed by the glycogen assay kit at 48 hpf. The amount of glycogen (ng/µl) was significantly less in I9E10*gaa* rescued morphants, compared to non-rescued I9E10*gaa*-MO morphants (I9E10*gaa*-MO + *gaa* mRNA: 143.6 ± 0.731 vs I9E10*gaa*-MO: 155.3 ± 2.186; p=0.0071) (Figure 3D).

In summary, the rescue experiment showed that embryos with correct morphology were more than non rescued embryos at 24 hpf, and at 48 hpf, although at the latter stage growth retardation or deformities did not differ. Glycogen amount was also significantly less in rescued morphants.

3-Bromopyruvate (3-BrPA) treatment

3-BrPA enhanced motility behavior in *gaa* morphants

The touch evoked response test, performed at 3 dpf on 3-BrPA-treated ATG*gaa* and I9E10*gaa* morphants, showed an improvement of escape contractions in both morphants (I9E10*gaa*-MO: n=20/30; ATG*gaa*-MO: n=24/33) compared to untreated morphants (n=30/30) (Supplementary Video 3 and Supplementary Figure 8).

3-BrPA improved muscle morphology in morphants

In transverse and longitudinal semi thin sections of ATG*gaa* and I9E10*gaa* morphants at 4 dpf treated with 3-BrPA, the space surrounding muscle fibres appeared either reduced compared to untreated morphants, as shown in toluidine blue-stained semi thin sections (Figure 4A, D) or devoid of positive fuchsia material, as shown in PAS-stained sections (Figure 4B, E).

At the electron microscopy level reduction in glycogen particles and presence of empty spaces around fibres was observed in both ATG*gaa* and I9E10*gaa* 3-BrPA-treated morphants (Figure 4C, F).

3-BrPA increased lysosomal content in morphants

Quantitation of LysoTracker (Figure 5A) red signal showed a significant increase in the red signal in ATG*gaa* morphants treated with 100 µM 3-BrPA, compared to untreated ATG*gaa*-MO (ATG*gaa*-MO + 3-BrPA: 45910 ± 8922 vs ATG*gaa*-MO: 12360 ± 3195; p=0.0011), as well as in I9E10*gaa*-MO treated morphants compared to untreated (I9E10*gaa*-MO + 3-BrPA: 15590 ± 3575 vs I9E10*gaa*-MO: 6070 ± 837.0; p=0.0175) (Figure 5B).

Quantitation of 2-NBDG showed in both 3-BrPA-treated morphants a significant decrease in the signal compared to untreated morphants (ATG*gaa*-MO + 3-BrPA: 3300 ± 377.0 vs ATG*gaa*-MO: 5261± 702.7; p=0.0200; I9E10*gaa*-MO + 3-BrPA: 2470 ± 217.2 vs I9E10*gaa*-MO: 6077 ± 851.9; p<0.0001) (Figure 5C).

Tracking *in vivo* of lysosomes and glycogen by fluorescent dyes showed an increase in lysosome content and a decrease in glycogen in both morphants after 3-BrPA treatment.

3-BrPA treatments improved rescue in I9E10*gaa* morphants

3-BrPA treatments were assessed after rescue in I9E10*gaa* morphants as the rescue experiment was carried out only in those embryos. At 24 hpf a significant increase in the number of embryos presenting with correct morphology was observed in morphants rescued with *gaa* mRNA and treated with 3-BrPA compared to untreated and rescued

morphants (I9E10*gaa*-MO + mRNA + 3-BrPA: 25.670 ± 1.856 vs I9E10*gaa*-MO + mRNA: 15.00 ± 2.082; p=0.0187); or compared to untreated morphants (I9E10*gaa*-MO + mRNA + 3-BrPA: 25.670 ± 1.856 vs I9E10*gaa*-MO: 7.333 ± 0.882; p=0.0009). Furthermore, the number of embryos presenting correct morphology was increased in I9E10*gaa*-MO + 3-BrPA compared to I9E10*gaa*-MO embryos (I9E10*gaa*-MO + 3-BrPA: 16.00 ± 2.082 vs I9E10*gaa*-MO: 7.333 ± 0.8819; p=0.0186) (Figure 6Aa, Ab).

Numbers of embryos showing growth retardation were not significantly different between groups (I9E10*gaa*-MO, rescued I9E10*gaa*-MO, and rescued I9E10*gaa*-MO + 3-BrPA). In the rescued morphants treated with 3-BrPA, those carrying deformities were significantly fewer than in the non-rescued and untreated morphants (I9E10*gaa*-MO: 11.67 ± 1.202 vs I9E10*gaa*-MO + mRNA + 3-BrPA: 3.667 ± 1.856; p=0.0224), but similar to the rescued morphants (I9E10*gaa*-MO + mRNA + 3-BrPA: 1.667 ± 0.8819 vs I9E10*gaa*-MO + mRNA: 2.333 ± 1.856; p=0.7619). The embryos treated with 3-BrPA alone presented a significant lower number of embryos carrying deformities than I9E10*gaa* morphants (I9E10*gaa*-MO + 3-BrPA: 4.667 ± 0.3333 vs I9E10*gaa*-MO: 11.67 ± 1.202; p=0,0050) (Figure 6Ac).

At 48 hpf, the number of morphants with correct morphology was significantly higher in the rescued morphants and 3-BrPA-treated compared to untreated and rescued morphants (I9E10*gaa*-MO + mRNA + 3-BrPA: 33.00 ± 3.215 vs I9E10*gaa*-MO + mRNA: 18.67 ± 3.667; p=0.0424), or compared to untreated and non-rescued morphants (I9E10*gaa*-MO + mRNA + 3-BrPA: 33.00 ± 3.215 vs I9E10*gaa*-MO: 11.00 ± 2.646; p=0.0062) (Figure 6Bb). Differences in growth retardation and in deformities were not significant between groups at 48 hpf (Figure 6Ad, Af).

3-BrPA treatment of rescued I9E10gaa morphants significantly reduced numbers of embryos presenting cardiac edema and hindbrain IV ventricle enlargement, at 48 hpf, compared to untreated morphants (Figure 6B,C). In particular, in rescued and 3-BrPA-treated morphants, numbers of embryos presenting cardiac edema were significantly fewer (2,2%, n=78) than in untreated and non-rescued morphants (20,3%, n=59); moreover, hindbrain enlargement was totally absent (0%, n=78) compared to untreated and non-rescued morphants (7,5%, n=59). Moreover, morphants treated with 3-BrPA alone showed a significant decrease (2,7%, n=62) in embryos percentage presenting cardiac edema and hindbrain IV ventricle enlargement, compared to untreated and non-rescued morphants (20,3%, n=59).

3-BrPA treatment of rescued I9E10*gaa* morphants did not change glycogen amount, at 48 hpf, compared to untreated and rescued I9E10*gaa* morphants (I9E10*gaa*-MO + mRNA +

3-BrPA: 139.2 ± 0.441 vs I9E10*gaa*-MO + mRNA: 143.6 ± 0.731; p=0.064). The 3-BrPA treatment alone reduced glycogen amount significantly, compared to the glycogen present in I9E10*gaa* morphants (I9E10*gaa*-MO + 3-BrPA: 0.1420 ± 0.001528 vs I9E10*gaa*-MO: 0.1487 ± 0.001202; p=0,0265) (Figure 6D).

In summary, 3-BrPA treatment improved the overall morphology and the cardiac edema in I9E10*gaa* morphants either alone or in addition to rescue. The rescue of I9E10*gaa* embryos reduced glycogen amount, in a comparable manner to 3-BrPA treatment.

3-BrPA treatment modified the expression of Beclin1, p62, and Lc3b transcripts and proteins

3-BrPA treatment did not significantly change *atg7, atg4, mTor, p62, lc3b* or *ulk1* transcripts levels in ATG*gaa* morphants and STD-Ctrl embryos compared to untreated.

3-BrPA-treatment significantly increased transcript levels of *lc3b* (I9E10*gaa*-MO + 3-BrPA: 3.298 ± 0.1572 vs I9E10*gaa*-MO: 2.284 ± 0.2973, p=0.0235), and *p62* (I9E10*gaa*-MO + 3-BrPA: 5.593 ± 0.6959 vs I9E10*gaa*-MO: 1.009 ± 0.07910, p=0.0006), and significantly decreased transcript levels of *beclin1* (I9E10*gaa*-MO + 3-BrPA: 0.3567 ± 0.2024 vs I9E10*gaa*-MO: 1.024 ± 0.1364, p=0.0357) in I9E10*gaa* morphants compared to untreated I9E10*gaa* morphants (Figure 7A).

A significant decrease in *beclin1* mRNA level was also observed in 3-BrPA-treated STD-Ctrl embryos compared to untreated STD-Ctrl embryos (STD-Ctrl + 3-BrPA: 0.341 ± 0.04 vs STD-Ctrl: 1.015 ± 0.102; p=0.0008).

3-BrPA-treatment significantly decreased Beclin1 protein amount in I9E10*gaa* morphants compared to untreated I9E10*gaa* morphants (I9E10*gaa*-MO: 0.9767 ± 0.1014 vs I9E10*gaa*-MO + 3-BrPA: 0.4833 ± 0.04096; p=0.0107).

3-BrPA-treatment significant increased p62 protein amount (STD-Ctrl + 3-BrPA: 0.6133 ± 0.01202 vs STD-Ctrl: 0.2733 ± 0.05925; p=0.0049) and significantly decreased Lc3b (STD-Ctrl + 3-BrPA: 1.117 ± 0.06489 vs STD-Ctrl: 0.8600 ± 0.05568; p=0.0399) in STD-Ctrl embryos compared to untreated STD-Ctrl (Figure 7B).

3-BrPA treatment main effect was an increase in *p62* and a decrease in *beclin1* mRNA levels and Beclin1 protein amount in I9E10*gaa* morphants. It also induced a decrease in *beclin1* mRNA, and an increase in p62 and decrease in Lc3b protein amount in STD-Ctrl.

DISCUSSION

Currently, the standard of care for Pompe disease patients is ERT which is efficacious in improving cardiomyopathy but not equally effective in cases with involvement of skeletal muscle: therefore, improved or supplementary therapeutic strategies are needed.

In our study, we have generated and characterized a new transient Pompe disease zebrafish model aimed at testing novel potential remedies for this pathology.

Taking advantage of two different morpholinos, one directed against the translation start site of the *gaa* transcript, and one targeting the splice site between intron 9 and exon 10, close to the catalytic site of the protein, we obtained the ATG*gaa* morphants, expressing low amount of the Gaa protein, and the I9E10*gaa* morphants, in which an aberrant *gaa* transcript and protein is present. Such aberrant protein, of theoretically lower molecular weight (57-58 kDa, compared to circa 70 kDa WT), was not detected by western blot. We presume that this truncated form deriving from the translation of the aberrant mRNA with intron retention in I9E10*gaa* morphants, acts as a dominant negative. Although the aberrant cDNA is clearly visible, as shown in Supplementary Figure 4B, the anti-Gaa antibody cannot possibly detect a truncated version of the protein, as the only conserved epitope in zebrafish is located at the C-terminus of the protein.

Our extensive investigation shows that several pathological characteristics recapitulate Pompe disease features [47] in both models, but especially in the I9E10*gaa*-MO-injected embryos.

We found an increase in glycogen content, detected using two different methods: one based on injection of 2-NBDG, that allows visualization of the glucose flux in 24 hpf zebrafish embryos by fluorescence microscopy analysis [48]; and one based on colorimetric analysis with a commercial assay kit tailored to our animal model. Both approaches showed a significant increment in glycogen amount in Pompe disease zebrafish knockdown models, more evident in the I9E10*gaa* morphants. The increment was rescued by co-injection with *gaa* mRNA confirming that Gaa deficiency was the cause of glycogen increase. These data were confirmed also by the morphological studies at optical and ultrastructural level.

We observed heart edema in almost half of the embryos among the I9E10gaa morphants at 48 hpf, that we associated with the Pompe disease phenotype. This was confirmed by the morphological analysis of the heart of 4 dpf glutaraldehyde-fixed morphants and control embryos. In I9E10gaa morphants, compared to controls, we observed

an increase in glycogen surrounding the pericardial muscles fibers and an increased amount of fluid in the pericardial cavity (edema), likely caused by the malfunction of the pericardial muscles. Moreover, morphants showed an abnormal deposition of the cardiac jelly layer, located between endocardium and myocardium [49]. Cardiac failure is the main cause of death in untreated classic infantile Pompe disease, but is also a characteristic of some late onset Pompe disease patients [50]. Edema of the heart, in some cases, has been associated to off target effects of morpholino in zebrafish. However, in our model, the edema was proportionate to the severity of the phenotypes and, importantly, *gaa* reintroduction during the rescue experiment ameliorated this particular aspect confirming that Gaa deficiency was the exclusive cause of the edema.

Furthermore, we observed reduced morphant motility, more marked in the I9E10*gaa* morphants, due to altered functionality of embryo muscles. This aspect was recovered during the rescue experiment, again confirming that Gaa deficiency, with consequent increment of glycogen storage, was the cause of the failed touch evoked response test.

Finally, in our knockdown model, we also found altered expression of autophagy-related components. In particular, we observed an increase in lysosomal corpuscles at ultrastructural level, a significant increase in lysosomal content (by LysoTracker staining), and a significantly increased expression of autophagy-related transcripts and proteins, with some differences between the two morphants.

The wide spectrum of Pompe disease is indeed attributed to altered autophagic flux, although it remains unclear how, since it is yet unknown if an excessive acceleration or reduction of this process is present. In addition to being involved in degradation, autophagy plays an important part in inflammation and pathogen clearance, and is implicated in cellular architectural changes that occur during differentiation and development [51]. Since autophagy is a fundamental evolutionarily conserved mechanism, and zebrafish development is strongly connected with it [35,52], we associated the developmental retardation, more evident in our I9E10*gaa* morphants, to altered autophagy [53]. Indeed, we observed significant changes in *beclin1* and *lc3b* transcript levels and in p62 and Lc3b protein levels in the I9E10*gaa* morphants. All these proteins are involved in early stages of autophagy: Beclin1 is an autophagy regulator involved in the formation of a double-membrane structure that engulfs cytoplasmic material to form the autophagosome [54], Lc3b is related to the crescent-shaped double membrane tightly associated to Beclin1, and p62 facilitates ubiquitinated protein degradation by linking the ubiquitin–proteasome system to the autophagy pathway [55]. The lack of correlation between

protein levels and mRNA expression is not surprising given that multiple processes contribute to the expression level of a protein [56].

All together our data confirm that knocking down or inducing the insertion of intron 10 in the *gaa* transcript in zebrafish, recapitulate most aspects of the human Pompe disease condition, which are more evident in the I9E10*gaa* morphants.

Remarkably, the zebrafish Pompe disease knockdown model, allowed us to evaluate the effects of 3-BrPA *in vivo*. This compound has never been tested before for Pompe disease. Since the main action of this compound is the inhibition of the key glycolytic enzyme HKII, a key regulator of glycolysis through autophagy [57], we hypothesized that 3-BrPA could potentially modulate glycogen accumulation and autophagy in Pompe disease muscle. The beneficial, but also toxic effects of this compound have been known in the last 10 years in particular for the treatment of glycolysis-dependent tumors [58,59]. In cancer cells, 3BrPA can accomplish its deleterious effect thanks to their high expression of monocarboxylate transporters and exacerbation of glycolytic metabolism [60]; however, 3-BrPA is slightly toxic to cells due to ROS production [61]. To limit such potential adverse effect, we used 3-BrPA at a concentration (100 µM) that was one-twentieth the concentration (2 mM) identified as LD_{50}.

We observed an improvement in morphants motility after 3-BrPA administration, which we interpreted as due to an improved functionality of embryo muscles, consistent with the decrease in glycogen storage. These data were confirmed also by the morphological studies at optical and ultrastructural level. In addition to its positive action in the I9E10*gaa* morphants, 3-BrPA enhanced the effect of the rescue experiment on glycogen storage, cardiac edema and hindbrain enlargement. Such result suggests that 3-BrPA can correct some of the phenotypic changes seen in the Pompe disease model and could be an adjuvant therapy in combination with ERT since the rescue experiment could mirror in some way the enzymatic replacement therapy.

Furthermore, 3-BrPA treatment induced changes in autophagy-related transcripts and proteins. To this regard, a major result of the treatment was the reduction in Beclin1 transcript and protein, since Beclin1 is central in the early formation of autophagosomes. A reduced nucleation, consequent to Beclin1 decrease, would produce fewer autophagosomes. The subsequent increase in Lc3b and p62 levels instead, is probably related to a slow down of the autophagic flux and to an increment in size of the autophagosomes.

We also observed an increment in red dots in the LysoTracker dye experiment in I9E10*gaa* morphants after 3-BrPA treatment, resulting in an increase in lysosomes, compared to untreated morphants. 3-BrPA is likely to induce a mild status of starvation that would activate the transcription factor EB (TFEB), the lysosomal biogenesis transcription factor, thereby increasing lysosomal activity (acidification and delivery of hydrolases) and trafficking (autophagosome - lysosome fusion) in strict correlation with autophagy [62].

In conclusion, we characterized for the first time a Pompe disease transient model in zebrafish that recapitulates most of the defects observed in human patients and reflects the genetic condition of most Pompe patients, in which the GAA is dysfunctional, but not totally absent.

This model thus has proven to be a suitable, rapid and low cost tool both for investigating pathogenic mechanisms of Pompe disease and for testing compounds with therapeutic potential. To this regard we have demonstrated, as proof of principle, that 3-BrPA has beneficial effects in the zebrafish Pompe disease model, since it reduces the glucose entrance in muscle cells and modulates the autophagy flux, without creating a problematic condition of starvation. Additional studies will be needed in a stable zebrafish mutant to explore 3-BrPA treatment for a long period of time. The present study is in fact preparatory to the development of a stable zebrafish PD model. In such model the catalytic site of the Gaa protein will be disrupted to better reproduce the pathological features of PD, keeping in mind that a compensation of the pathological phenotype could occur in adult stages, as already reported [63].

Our new zebrafish PD model, will simplify testing novel drugs with therapeutic potential, as 3-BrPA, reducing timing and costs of the screening. Moreover, this translational model, that recapitulates better the patient conditions, will accelerate further investigations that underlies glycogen storage conditions.

Acknowledgements

The authors are grateful to the “Associazione Italiana Glicogenosi (AIG)” and Pompe disease patients for support and inspiration. We thank Dr. Renato Bacchetta for helping with histology.

Author contributions

Conceived and designed the experiments: C.B. and S.C.; performed the experiments: C.B., F.B., F.S. and A.Br.; analyzed the data: C.B., S.C. and M.M.; contributed reagents/materials/analysis tools: M.M., L.M. and R.M.; wrote the paper: C.B. and M.M.; made critical revision of the manuscript for important intellectual content: M.B., A.B. and S.C.

Conflict of Interest statement

None declared.

REFERENCES

1. Kohler L, Puertollano R, Raben N. Pompe Disease: From Basic Science to Therapy. *Neurotherapeutics.* 2018;15:928–942.
2. Engel AG, Hirschhorn R, Huie ML. In: Engel A, Franzini-Armstrong C, eds. *Acid Maltase Deficiency*. New York, New York, USA: McGraw-Hill; 2004:1559-1586.
3. Güngör D, Reuser AJJ. How to describe the clinical spectrum in Pompe disease? *Am J Med Genet*. 2013;161:399–400.
4. Raben N, Danon M, Gilbert AL, Dwivedi S, Collins B, Thurberg BL, et al. Enzyme replacement therapy in the mouse model of Pompe disease. *Mol Genet Metab.* 2003;80:159–169.
5. Van den Hout JM, Kamphoven JH, Winkel LP, Arts WF, De Klerk JB, Loonen MC, et al. Long-term intravenous treatment of Pompe disease with recombinant human alpha-glucosidase from milk. *Pediatrics*. 2004;113:448–457.
6. Schoser B, Hill V, Raben N. Therapeutic approaches in glycogen storage disease type II/Pompe disease. *Neurotherapeutics.* 2008;5:569–578.

7. Chen LR, Chen CA, Chiu SN, Chien YH, Lee NC, Lin MT, et al. Reversal of cardiac dysfunction after enzyme replacement in patients with infantile-onset Pompe disease. *J Pediatr.* 2009;155:271–275.
8. Strothotte S, Strigl-Pill N, Grunert B, Kornblum C, Eger K, Wessig C, et al. Enzyme replacement therapy with alglucosidase alfa in 44 patients with late- onset glycogen storage disease type 2: 12-month results of an observational clinical trial. *J Neurol.* 2010;257:91–97.
9. Fukuda T, Roberts A, Ahearn M, Zaal K, Ralston E, Plotz PH, et al. Autophagy and lysosomes in Pompe disease. *Autophagy*. 2006;2: 318–320.
10. Thurberg BL, Lynch Maloney C, Vaccaro C, Afonso K, Tsai AC, Bossen PS, et al. Characterization of pre- and post-treatment pathology after enzyme replacement therapy for Pompe disease. *Lab Invest.* 2006;86:1208-1220.
11. Cardone M, Porto C, Tarallo A, Vicinanza M, Rossi B, Polishchuk E, et al. Abnormal mannose-6-phosphate receptor trafficking impairs recombinant alpha-glucosidase uptake in Pompe disease fibroblasts. *Pathogenetics*. 2008;1:6.
12. Van der Ploeg AT, Reuser AJJ. Pompe's disease. *Lancet.* 2008;372:1342–1353.
13. Levine B and Klionsky DJ. Development by self-digestion: molecular mechanisms and biological functions of autophagy. *Dev Cell.* 2004;6:463–477.
14. Mizushima N, Levine B. Autophagy in mammalian development and differentiation. *Nat Cell Biol.* 2010;12:823–830.
15. Lee DL, Bareja A, Bartlett DB, White JP. Autophagy as a Therapeutic Target to Enhance Aged Muscle Regeneration. *Cells*. 2019;8:183.
16. Raben N, Roberts A, Plotz PH. Role of autophagy in the pathogenesis of Pompe disease. *Acta Myol.* 2007;26:45-48.
17. Kishnani PS and Beckemeyer AA. New therapeutic approaches for Pompe disease: enzyme replacement therapy and beyond. *Pediatr Endocrinol Rev.* 2014;1:114-124.
18. McCall AL, Stankov SG, Cowen G, Cloutier D, Zhang Z, Yang L, et al. Reduction of Autophagic Accumulation in Pompe Disease Mouse Model Following Gene Therapy. *Curr Gene Ther.* 2019;19(3):197-207.
19. Lim JA, Yi H, Gao F, Raben N, Kishnani PS, Sun B. Intravenous Injection of an AAV-PHP.B Vector Encoding Human Acid α-Glucosidase Rescues Both Muscle and CNS Defects in Murine Pompe Disease. *Mol Ther Methods Clin Dev.* 2019;12: 233–245.

20. Takikita S, Schreiner C, Baum R, Xie T, Ralston E, Plotz PH, et al. Fiber Type Conversion by PGC-1α Activates Lysosomal and Autophagosomal Biogenesis in Both Unaffected and Pompe Skeletal Muscle. *PLoS One*. 2010;5(12):e15239.
21. Martina JA, Diab HI, Lishu L, Jeong-A L, Patange S, Raben N, et al. The Nutrient-Responsive Transcription Factor TFE3, Promotes Autophagy, Lysosomal Biogenesis, and Clearance of Cellular Debris. *Sci Signal*. 2014;7(309): ra9.
22. Geschwind JH, Ko YH, Torbenson MS, Magee C, Pedersen PL. Novel Therapy for Liver Cancer: Direct Intraarterial Injection of a Potent Inhibitor of ATP. *Cancer Res.* 2002;62:3909-3913.
23. Pelicano H, Martin DS, Xu R-H, Huang P. Glycolysis inhibition for anticancer treatment. *Oncogene*. 2006;25:4633–4646.
24. Zhang Q, Zhang Y, Zhang P, Chao Z, Xia F, Jiang C, et al. Hexokinase II inhibitor, 3-BrPA induced autophagy by stimulating ROS formation in human breast cancer cells. *Genes & Cancer.* 2014;5:3-4.
25. Graziano F, Ruzzo A, Giacomini E, Ricciardi T, Aprile G, Loupakis F, et al. Glycolysis gene expression analysis and selective metabolic advantage in the clinical progression of colorectal cancer. *Pharmacogenomics J*. 2017;17:258-264.
26. Ganapathy-Kanniappan S, Geschwind JF, Kunjithapatham R, Buijs M, Syed LH, Rao PR, et al. 3-Bromopyruvate induces endoplasmic reticulum stress, overcomes autophagy and causes apoptosis in human HCC cell lines. *Anticancer Res.* 2010;30:923-935.
27. Davidescu M, Sciaccaluga M, Macchioni L, Angelini R, Lopalco P, Rambotti MG, et al. Bromopyruvate mediates autophagy and cardiolipin degradation to monolyso-cardiolipin in GL15 glioblastoma cells. *J Bioenerg Biomembr*. 2012;44:51-60.
28. Tsai HJ, Wilson JE. Functional organization of mammalian hexokinases: both N- and C-terminal halves of the rat type II isozyme possess catalytic sites. *Arch Biochem Biophys.* 1996;329:17–23.
29. Ko YH, Pedersen PL, Geschwind JF. Glucose catabolism in the rabbit VX2 tumor model for liver cancer: characterization and targeting hexokinase. *Cancer Lett*. 2001;173:83–91.
30. Pedersen PL. Warburg, me and Hexokinase 2: Multiple discoveries of key molecular events underlying one of cancers' most common phenotypes, the "Warburg Effect", i.e., Elevated glycolysis in the presence of oxygen. *J Bioenerg Biomembr.* 2007;39: 211–222.

31. Queiros O, Preto A, Pacheco A, Pinheiro C, Azevedo-Silva J, Moreira R, et al. Butyrate activates the monocarboxylate transporter MCT4 expression in breast cancer cells and enhances the antitumor activity of 3-bromopyruvate. *J Bioenerg Biomembr*. 2012;44:141–153.
32. Halestrap AP, Price NT. The proton-linked monocarboxylate transporter (MCT) family: structure, function and regulation. *Biochem J.* 1999;343:281–299.
33. Raben N, Nagaraju K, Lee E, Kessler P, Byrne B, Lee L, et al. Targeted Disruption of the Acid α-Glucosidase Gene in Mice Causes an Illness with Critical Features of Both Infantile and Adult Human Glycogen Storage Dis. Type II. *J Biol Chem*. 1998; 73(30):19086-19092.
34. Hiniker A, Margeta M. Skeletal myopathy in Pompe disease: a failure of satellite cell activation? *Acta Neuropathol Commun.* 2018; 6(1):133
35. Varga M, Fodor E, Vellai T. Autophagy in zebrafish. *Methods*. 2015;75:172-180.
36. Mathai BJ, Meijer AH, Simonsen A. Studying Autophagy in Zebrafish. *Cells*. 2017;6(3):E21.
37. González-Alvarez R, Ortega-Cuellar D, Hernández-Mendoza A, Moreno-Arriola E, Villaseñor-Mendoza K, Gálvez-Mariscal A, et al. The hexokinase gene family in the zebrafish: Structure, expression, functional and phylogenetic analysis. *Comp Biochem Physiol B Biochem Mol Biol.* 2009;152(2):189-195.
38. Omlin T, Weber JM. Exhausting exercise and tissue-specific expression of monocarboxylate transporters in rainbow trout. *Am J Physiol Regul Integr Comp Physiol.* 2013;304(11):R1036-1043.
39. Nasevicius A, Ekker SC. Effective targeted gene ‘knockdown’ in zebrafish. *Nat Genet.* 2000;26:216–220.
40. Kimmel CB, Ballard WW, Kimmel ST, Ullmann B, Schilling TF. Stages of Embryonic Development of the Zebrafish. *Dev Dyn.* 1995;203:253-310.
41. He C, Klionsky DJ. Analyzing autophagy in zebrafish. *Autophagy*. 2010;6:642-644.
42. Schindelin J, Arganda-Carreras I, Frise E, Kaynig V, Longair M, Pietzsch T, et al. Fiji: an open-source platform for biological-image analysis. *Nat Methods*. 2012;9:676–682.
43. Ro H, Soun K, Kim E, Rhee M. Novel Vector System Opimized for injecting in vitro-synthetized mRNA into zebrafish embryos. *Mol Cells.* 2004;17:373-376.
44. Shoshan MC. 3-bromopyruvate: Targets and outcomes. *J Bioenerg Biomembr.* 2012;44:7-15.

45. Granato M, van Eeden FJ, Schach U, Trowe T, Brand M, Furutani-Seiki M, et al. Genes controlling and mediating locomotion behavior of the zebrafish embryo and larva. *Development.* 1996;123:399–413.
46. Louzao MC, Espiña B, Vieytes MR, Vega FV, Rubiolo JA, Baba O, et al. ”Fluorescent glycogen" formation with sensibility for in vivo and in vitro detection. *Glycoconj J*. 2008;25(6):503-510.
47. Dasouki M, Jawdat O, Almadhoun O, Pasnoor M, McVey ML, Abuzinadah A, et al. Pompe disease: Literature Review and Case Series. *Neurol Clin*. 2014;32:751-779.
48. Tabassum N, Tai H, Jung D, Williams DR. Fishing for Nature’s Hits: Establishment of the Zebrafish as a Model for Screening Antidiabetic Natural Products. *Evid Based Complement Alternat Med*. 2015;2015:287847.
49. Lockhart M, Wirrig E, Phelps A, Wessels A. Extracellular Matrix and Heart Development. *Birth Defects Res A Clin Mol Teratol*. 2011;91:535-550.
50. Forsha D, Li JS, Smith PB, van der Ploeg AT, Kishnani P, Pasquali SK. Cardiovascular Abnormalities in Late Onset Pompe disease and Response to Enzyme Replacement Therapy for the Late Onset Treatment Study Investigators. *Genet Med*. 2011;13:625-631.
51. Ravikumar B, Sarkar S, Davies JE, Futter M, Garcia-Arencibia M, Green-Thompson ZW, et al. Regulation of mammalian autophagy in physiology and pathophysiology. *Physiol Rev*. 2010;90:1383-1435.
52. Agnello M, Bosco L, Chiarelli R, Martino C, Roccheri MC. The role of autophagy and apoptosis during embryo development. In Ntuli TM, eds. *Cell Death – Autophagy, Apoptosis and Necrosis.* Rijeka: Croatia: INTECH Press; 2015:83–112.
53. Miccoli A, Dalla Valle L, Carnevali O. The maternal control in the embryonic development of zebrafish. *Gen Comp Endocrinol.* 2017;245:55-58.
54. Kang R, Zeh HJ, Lotze MT, Tang D. The Beclin 1 network regulates autophagy and apoptosis. *Cell Death Differ.* 2011;18:571-580.
55. Liu WJ, Ye L, Huang WF, Guo LJ, Xu ZG, Wu HL, et al. p62 links the autophagy pathway and the ubiqutin-proteasome system upon ubiquitinated protein degradation. *Cell Mol Biol Lett*. 2016;21:29.
56. McManus J, Cheng Z, Vogel C. Next-generation analysis of gene expression regulation–comparing the roles of synthesis and degradation*. Mol Biosyst*. 2015;11:2680–2689.

57. Jiao L, Zhang HL, Li DD, Yang KL, Tang J, Li X, et al. Regulation of Glycolytic Metabolism by Autophagy in Liver Cancer Involves Selective Autophagic Degradation of HK2 (hexokinase 2). *Autophagy*. 2018;14:671-684.
58. Birsoy K, Wang T, Possemato R, Yilmaz OH, Koch CE, Chen WW, et al. MCT1-mediated transport of a toxic molecule is an effective strategy for targeting glycolytic tumors. *Nat Genet*. 2013;45:104–110.
59. Ehrke E, Arend C, Dringen R. 3-Bromopyruvate Inhibits Glycolysis, Depletes Cellular Glutathione, and Compromises the Viability of Cultured Primary Rat Astrocytes. *J Neurosci Res*. 2015;93:1138-1146.
60. Azevedo-Silva J, Queirós O, Baltazar F, Ułaszewski S, Goffeau A, Ko YH, et al. The anticancer agent 3-bromopyruvate: a simple but powerful molecule taken from the lab to the bedside. *J Bioenerg Biomembr.* 2016;48:349–362.
61. Macchioni L, Davidescu M, Roberti R, Corazzi L. The energy blockers 3-bromopyruvate and lonidamine: effects on bioenergetics of brain mitochondria. *J Bioenerg Biomembr.* 2014;46:389–394.
62. Xu H, Ren D. Lysosomal Physiology. *Annu Rev Physiol*. 2015;77:57-80.
63. Wu J, Yang Y, Sun C, Sun S, Li Q, Yao Y, et al. Disruption of the gaa Gene in Zebrafish Fails to Generate the Phenotype of Classical Pompe Disease. *DNA and cell biol*. 2017;36:10–17.

Figure 1.

***gaa* zebrafish morphants recapitulate the human Pompe disease phenotype. (A)** Classes of phenotypes shown for the I9E10*gaa*-injected embryos (C1, C2 and C3). In morphants belonging to class C2, features such as cardiac edema (red asterisk), enlargement of the IV cerebral ventricle (black arrowhead) or both alterations are visible. Morphants of the class C1 appear normal, while those of class C3 show disrupted morphology. Scale bar = 300 µm. **(B)** Percentages of classes obtained with ATG*gaa* and I9E10*gaa* morpholinos injections. **(C)** Glycogen amount measured by the Glycogen Assay kit II in ATG*gaa*-MO and I9E10*gaa*-MO morphants pertaining to the C1 class. Results were achieved from 4 independent experiments, each using 10 embryos pulled together, for a total of 40 embryos per group. **(D, upper panel)** Toluidine blue-stained transverse semithin sections of I9E10*gaa* morphants showing increased spaces surrounding muscle fibres (black arrows), not observed in STD-Ctrl embryos. Scale bar = 20 µm. **(D, lower panel)** PAS staining on transverse semithin sections of STD-Ctrl embryo, compared to I9E10*gaa* morphant at 4 dpf. Glycogen detected in spaces surrounding muscle fibers (black arrows) is increased and more visible in morphants, compared to controls. Scale bar = 2µm. **(E)** Electron micrographs showing increase in glycogen (black arrows) and lysosomal corpuscles (white arrowheads) in I9E10*gaa* morphants, but not in STD-Ctrl embryos. Scale bar = 2µm. **(F)** Toluidine blue-stained transverse semithin sections of STD-Ctrl embryo heart **(a)** compared to I9E10*gaa* morphant heart **(b)** at 4 dpf. Increased spaces surrounding pericardial muscle fibres (black arrows) and lipid droplets (black arrowhead) are present in morphants, but not in controls **(b'').** Moreover, an augment of the cardiac jelly layer (white arroheads) is observed in the morphant heart **(b'')**, with the presence of an increased cardiac fluid (asterisks) (**b**). Scale bar = 100 µm. **(G)** Quantitation of the LysoTracker red signal; and **(H)** of the 2-NBDG green signal in both morphants and in STD-Ctrl. Results were achieved from 5 independent experiments each using 25 ATG*gaa* morphants, 25 I9E10*gaa* morphants and 25 STD-Ctrl embryos.

Figure 2.

Expression of autophagy related transcripts and proteins. (A) *beclin1* and *lc3b* transcript levels at 48 hpf. Results were achieved from 5 independent experiments each using cDNA obtained after RNA extraction from 10 embryos pulled together, for a total of 50 embryos. **(B)** Representative western blot showing Beclin1, p62 and Lc3b protein

bands; and their quantitation (average of 3 gels) at 4 dpf, in I9E10*gaa* morphants compared to STD-Ctrl.

Figure 3.

Rescue of I9E10*gaa* morphants phenotype. (A) Classes of phenotypes obtained at 24 hpf after co-injection of I9E10*gaa*-MO (1 pmol/embryo) and 10pg/4nL *gaa* mRNA. **(B)** Graphs reporting average numbers of embryos with correct morphology **(a, b)**, developmental delay **(c, d)** and deformities **(e, f)** at 24 hpf and 48 hpf. The total number of embryos per group were: n=59 I9E10*gaa*-MO, n=73 rescued I9E10*gaa*-MO, n=78 3-BrPA rescued I9E10*gaa*-MO, n=62 I9E10*gaa*-MO plus 3-BrPA, n=60 STD Ctrl. **(C)** Representative phenotypes of STD-Ctrl, I9E10*gaa*-MO and I9E10*gaa* rescued embryos, at 2 dpf, with cardiac edema (black asterisks) and enlargement of IV hindbrain ventricle (white asterisks) more evident in I9E10*gaa* morphants. Scale bar = 200 µm. **(D)** Evaluation of glycogen amount in I9E10*gaa* morphants before and after rescue, compared to STD-Ctrl, at 48 hpf. Results were achieved from 4 independent experiments, each using 10 embryos pulled together, for a total of 40 embryos.

Figure 4.

Effect of 3-BrPA treatment on muscle morphology. (A, D) Toluidine blue- and **(B, E)** PAS-stained transverse semi thin sections of I9E10*gaa*-MO embryos at 4 dpf, showing that, after 3-BrPA treatment, spaces surrounding muscle fibres (arrows) appear either reduced or devoid of positive fuchsia material around muscle fibres. Scale bars = 20 µm. (**C**, **F**) Electron micrographs showing that glycogen particles (black arrows) present in I9E10*gaa* morphants (**C**), appear decreased after 3-BrPA treatment (F), while empty spaces around fibres (black arrowheads) appear increased. Lysosomal corpuscles (white arrowheads) are visible in untreated I9E10*gaa* morphants . Scale bar = 2µm.

Figure 5.

3-BrPA treatment effect on lysosomes. (A) Fluorescence images showing LysoTracker and 2-NBDG signals in STD-Ctrl **(a-c**), ATG*gaa*-MO injected embryos **(d-f)**, ATG*gaa*-MO 3-BrPA-treated embryos **(g-i)**, I9E10*gaa*-MO injected embryos **(j-l)**, I9E10*gaa*-MO 3-BrPA-treated embryos **(m-o)**. Scale bar = 100 µm. **(B, C)** Quantitation of LysoTracker and 2-NBDG signal in ATG*gaa* and I9E10*gaa* morphants before and after 3-BrPAtreatment, and in STD-Ctrl embryos. The LysoTracker dye and 2-NBDG assessment was performed in 23

zebrafish embryos per group (115 embryos in total), obtained from 5 independent experiments.

Figure 6.

3-BrPA treatment effect on rescue experiment. (A) Graphs reporting average numbers of embryos with correct morphology **(a, b)**, developmental delay **(c, d)** and deformities **(e, f)** at 24 hpf and 48 hpf, showing improvement of phenotypes after 3-BrPA-treatment in embryos either rescued or non rescued. The total number of embryos per group were: n=59 I9E10*gaa*-MO, n=73 rescued I9E10*gaa*-MO, n=78 3-BrPA rescued I9E10*gaa*-MO, n=62 I9E10*gaa*-MO plus 3-BrPA, n=60 STD Ctrl. **(B, C)** Percentages of I9E10*gaa* morphants presenting cardiac edema or hindbrain IV ventricle enlargement after rescue, after rescue plus 3-BrPA treatment, and after 3-BrPA alone. The total number of embryos per group were: n=59 I9E10*gaa*-MO, n=73 rescued I9E10*gaa*-MO, n=78 3-BrPA rescued I9E10*gaa*-MO, n=62 I9E10*gaa*-MO plus 3-BrPA. **(D)** Glycogen amount in I9E10gaa morphants, after rescue, after rescue plus 3-BrPA treatment, and after 3-BrPA alone. Results were achieved from 4 independent experiments, each using 10 embryos pulled together, for a total of 40 embryos per group.

Figure 7.

Effects of 3-BrPA on autophagy-related transcripts and proteins in I9E10*gaa* morphants.

(A) *beclin1, p62* and *lc3b* transcript levels; and **(B)** representative western blot showing Beclin1, p62 and Lc3b protein bands; and their quantitation (average of 3 gels) at 4 dpf, in in I9E10*gaa* morphants and STD-Ctrl embryos before and after 3-BrPA treatment. Results were achieved using cDNA obtained after RNA extraction from 10 embryos pulled together, collected during 5 independent experiments, for a total of 50 embryos.

Table 1.

Transcripts of genes related to autophagy were evaluated by qRT-PCR using primers reported in table 1, normalized to the reference gene mRNA (housekeeping gene).

Table 2.

List of primary and secondary antibodies used for the experiments described. Antibodies name, dilution used, catalog number and Lot number (where available) were included.

Table 1

Primers:

gaa-Forward	5'-AGTCAGCGAGCCCAGGAT-3'
gaa-Reverse	5'-CCAACGAAGCAGGAAACA-3'
atg4b-Forward	5’-ACACCACTCAGCCAGCAG-3’
atg4b-Reverse	5’-AAGCCAGCAGCAATAGAAGG-3’
beclin1-Forward	5’-GCCATTGTATTGTTCAGGTG-3’
beclin1-Reverse	5’-CAGAAGCCAGTGTCATCC-3’
atg7-Forward	5’-AGAGTCCAGTCCGATGTC-3’
atg7-Reverse	5’-GAAGTAACAGCCGAGACG-3’
p62-Forward	5’-TTTGGCTCTTGTGAAGGATGAC-3’
p62-Reverse	5’-GAGGGCTAAAGTGAGGTGTAGTGA-3’
mtor-Forward	5’-ATACGCATCCAGTCCATTG -3’
mtor-Reverse	5’-TCATTAGCCAGTAGAGTGTTC-3’
lc3b-Forward	5’-CCTCCAACTCAACTCCAACC-3’
lc3b-Reverse	5’-GCCGTCTTCGTCTCTTTCC-3’
Housekeeping gene:	
Ef1a-Forward	5’-CTGTACCTGTGGGTCGTGTGGAGACTG-3’
Ef1a-Reverse	5’-CAGCCTTCTGTGCAGACTTTGTGAC-3’

Primary antibodies	Dilution		Company	Cat. numb.	Lot
LC3B (NB100-2220)	1:500	polyclonal	Novus Biologicals Europe, Abingdon, UK	NB100-2220	Lot:EC
GAA	1:100	polyclonal	Sigma Aldrich, St. Louis, Missouri, USA	SAB2100872	Lot: QC14285
p62	1:500	polyclonal	PROGEN Biotechnik GmbH, Heidelberg, Germany	GP62-c	Lot:709151
mTOR	1:500	polyclonal	Santa Cruz Biotecnology, Santa Cruz, CA, USA	sc-8319	N/A*
p-mTOR	1:200	monoclonal	Santa Cruz Biotecnology, Santa Cruz, CA, USA	sc-293133	N/A*
AMPk	1:500	polyclonal	Santa Cruz Biotecnology, Santa Cruz, CA, USA	sc-25792	N/A*
pAMPk	1:200	polyclonal	Santa Cruz Biotecnology, Santa Cruz, CA, USA	sc-33524	N/A*
BECLIN1	1:500	polyclonal	Thermo Fisher, MA, USA	PA1-46454	Lot: #SC2360229A
αTubulin	1:1000	monoclonal	Sigma Aldrich, St. Louis, Missouri, USA	T7451	Lot:051M4770
LAMP2 (H4B4)	1:500	monoclonal	DSHB, Iowa, USA	H4B4	N/A

Secondary antibodies	Dilution		Company	Cat. numb.	Lot
Amersham ECL Goat anti-Rabbit IgG HRP	1:1000	polyclonal	GE Healtcare Lifescience, Chicago, IL, USA	NA9340V	Lot:16955624
Amersham ECL Goat anti-Mouse IgG HRP	1:1000	monoclonal	GE Healtcare Lifescience, Chicago, IL, USA	NA931V	Lot:16982037
Biotin-SP-conjugated AffiniPure Donkey Anti-Guinea Pig IgG (H+L)	1:1000	polyclonal	Jackson ImmunoResearch, Cambridgeshire, UK	706-065-148	Lot:106654

* kind gift from Dr. Giuseppina Caretti's Laboratory, Università degli studi di Milano;

+ Note that, except for the anti-LC3B antibody, validated in zebrafish (see i.e. Ran et al., 2017), all other antibodies had not been reported in the literature as cross-reacting with Danio rerio proteins. The choice of the right antibody was based on the epitope being at least 40% similar to the zebrafish one.

HIGHLIGHTS

1) A new transient Pompe disease zebrafish model has been generated and characterized;

2) Acid 3-Bromopyruvic (3-BrPA) improves some of defects seen in the PD model;

3) 3-BrPA represents a new promising compound for Pompe disease patients;

4) The zebrafish PD model will simplify testing novel drugs with therapeutic potential.

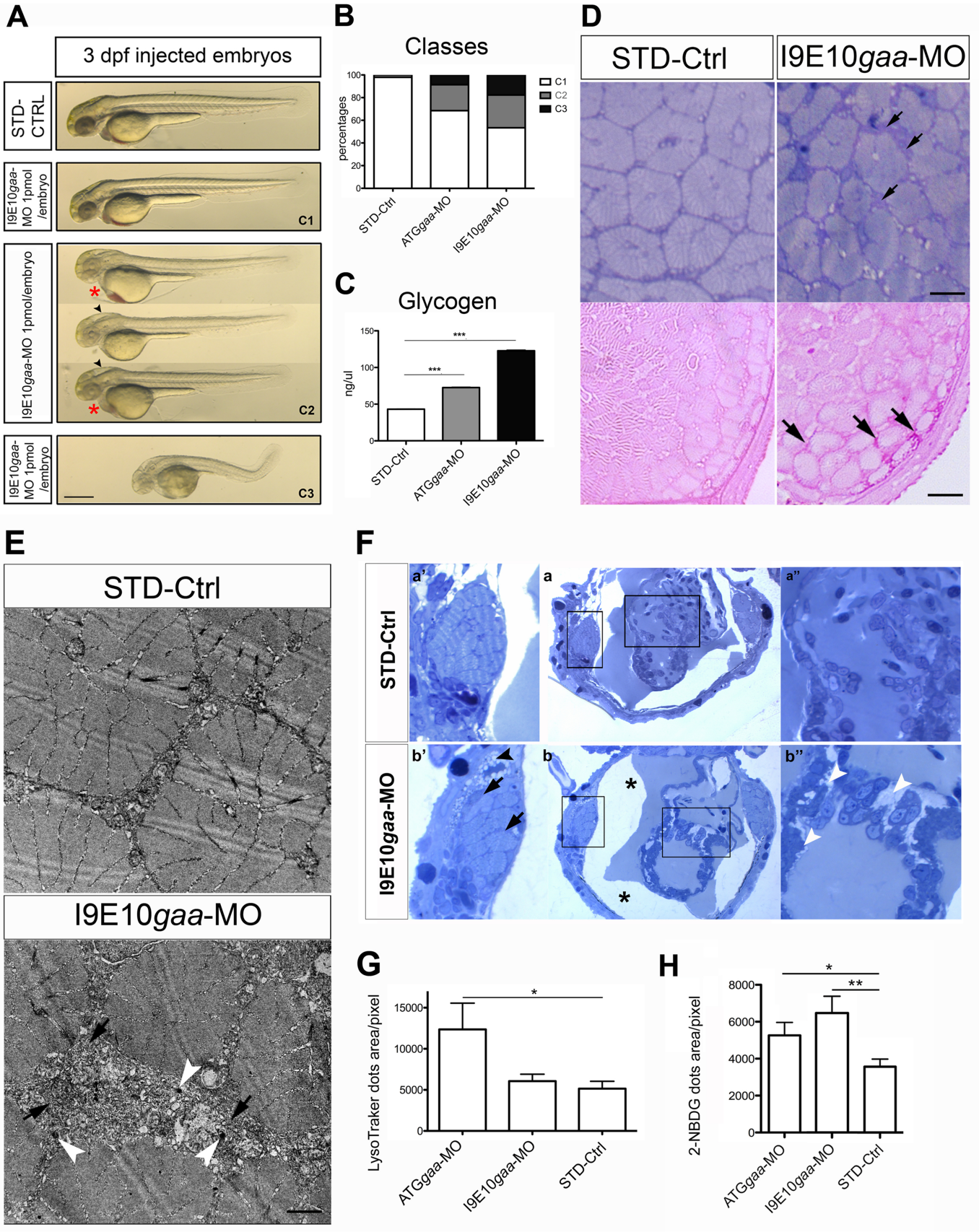
A
3 dpf injected embryos
STD-CTRL
I9E10gaa-MO 1pmol /embryo
C1
I9E10gaa-MO 1pmol/embryo
C2
I9E10gaa-MO 1pmol /embryo
C3
B
Classes
percentages
C1
C2
C3
STD-Ctrl
ATGgaa-MO
I9E10gaa-MO
C
Glycogen
ng/ul
***
***
STD-Ctrl
ATGgaa-MO
I9E10gaa-MO
D
STD-Ctrl
I9E10gaa-MO
E
STD-Ctrl
I9E10gaa-MO
F
STD-Ctrl
I9E10gaa-MO
a'
a
a''
b'
b
b''
G
LysoTraker dots area/pixel
*
ATGgaa-MO
I9E10gaa-MO
STD-Ctrl
H
2-NBDG dots area/pixel
*
**
ATGgaa-MO
I9E10gaa-MO
STD-Ctrl

Figure 1

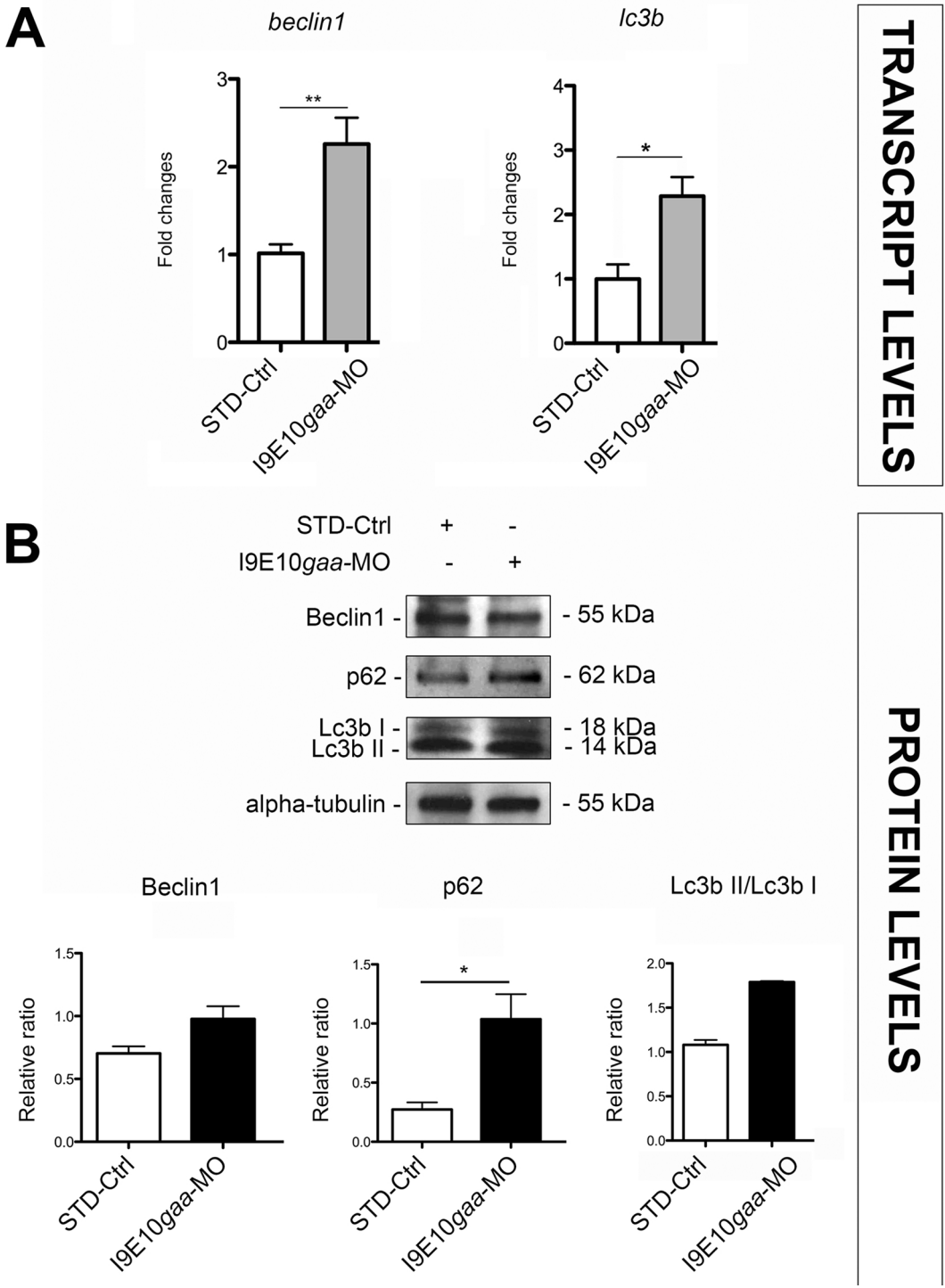
A
beclin1
lc3b
Fold changes
**
*
STD-Ctrl
I9E10gaa-MO
TRANSCRIPT LEVELS
B
STD-Ctrl + -
I9E10gaa-MO - +
Beclin1 - 55 kDa
p62 - 62 kDa
Lc3b I - 18 kDa
Lc3b II - 14 kDa
alpha-tubulin - 55 kDa
Beclin1
p62
Lc3b II/Lc3b I
Relative ratio
PROTEIN LEVELS

Figure 2

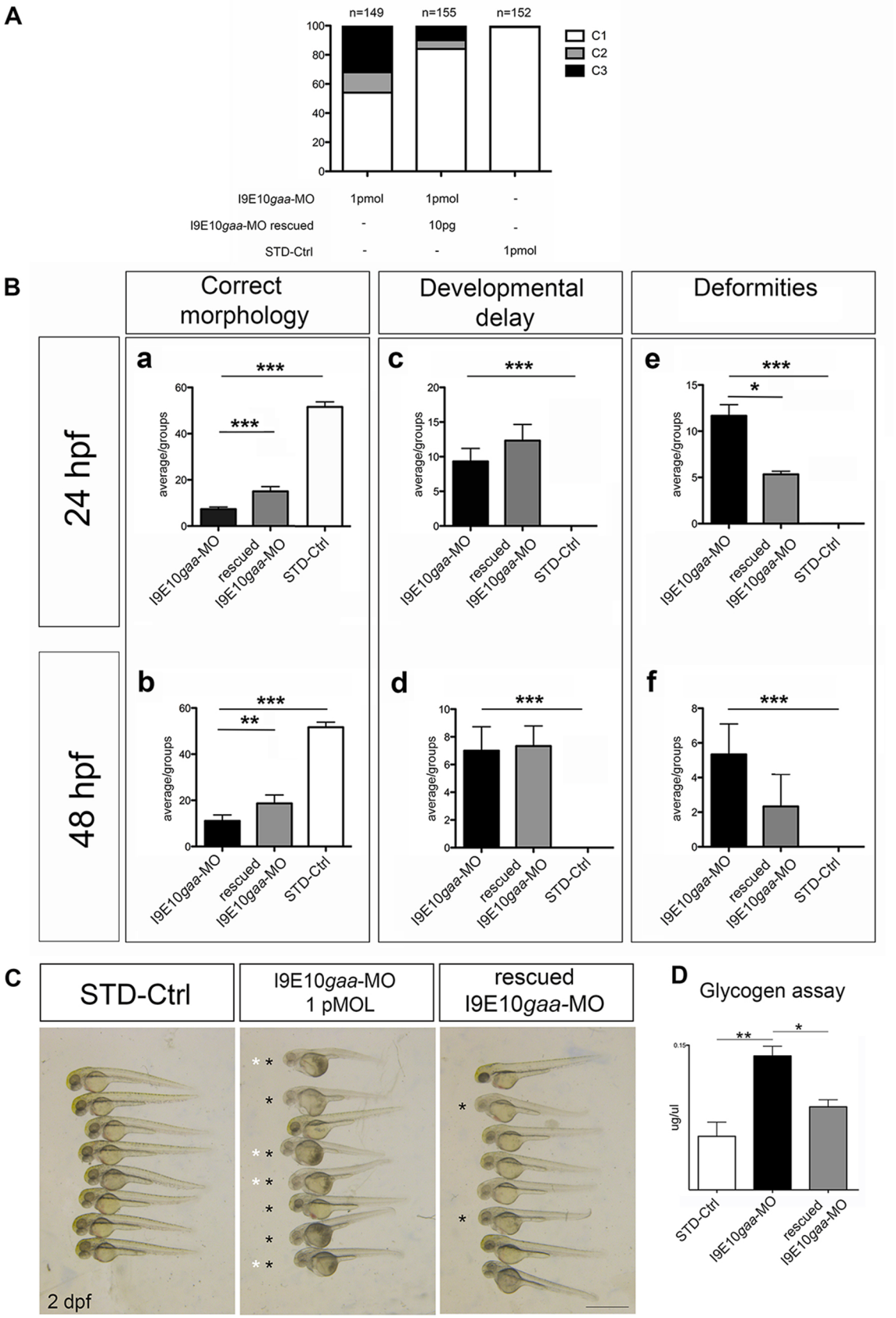
A
n=149
n=155
n=152
C1
C2
C3
I9E10gaa-MO 1pmol 1pmol -
I9E10gaa-MO rescued - 10pg -
STD-Ctrl - - 1pmol
B
Correct morphology
Developmental delay
Deformities
24 hpf
48 hpf
a
b
c
d
e
f
average/groups
I9E10gaa-MO
rescued I9E10gaa-MO
STD-Ctrl
C
STD-Ctrl
I9E10gaa-MO 1 pMOL
rescued I9E10gaa-MO
2 dpf
D
Glycogen assay
ug/ul

Figure 3

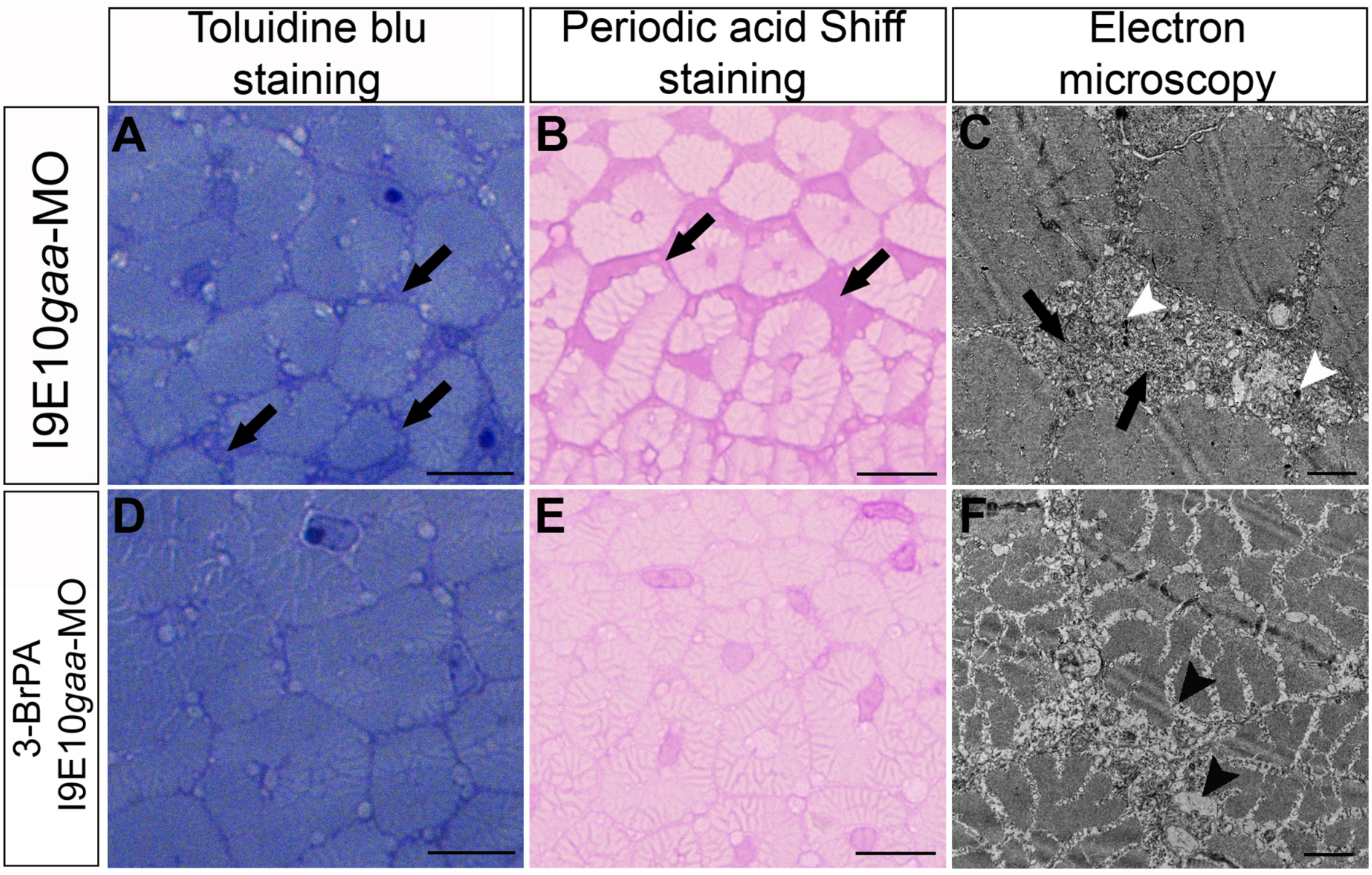
Toluidine blu staining
Periodic acid Shiff staining
Electron microscopy
I9E10gaa-MO
3-BrPA I9E10gaa-MO
A
B
C
D
E
F

Figure 4

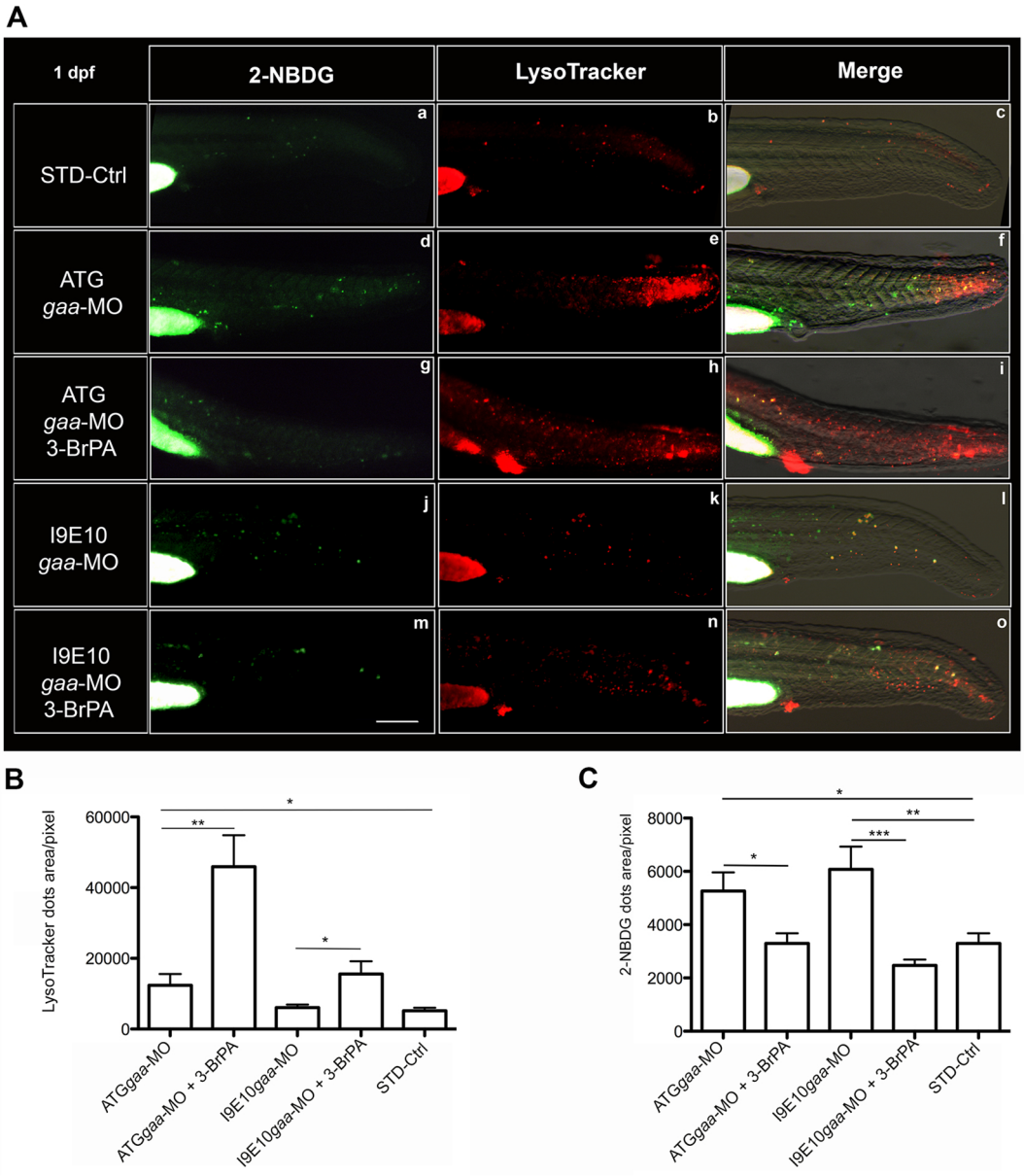
A
1 dpf
2-NBDG
LysoTracker
Merge
STD-Ctrl
ATG gaa-MO
ATG gaa-MO 3-BrPA
I9E10 gaa-MO
I9E10 gaa-MO 3-BrPA
a
b
c
d
e
f
g
h
i
j
k
l
m
n
o
B
LysoTracker dots area/pixel
60000
40000
20000
0
ATGgaa-MO
ATGgaa-MO + 3-BrPA
I9E10gaa-MO
I9E10gaa-MO + 3-BrPA
STD-Ctrl
C
2-NBDG dots area/pixel
8000
6000
4000
2000
0

Figure 5

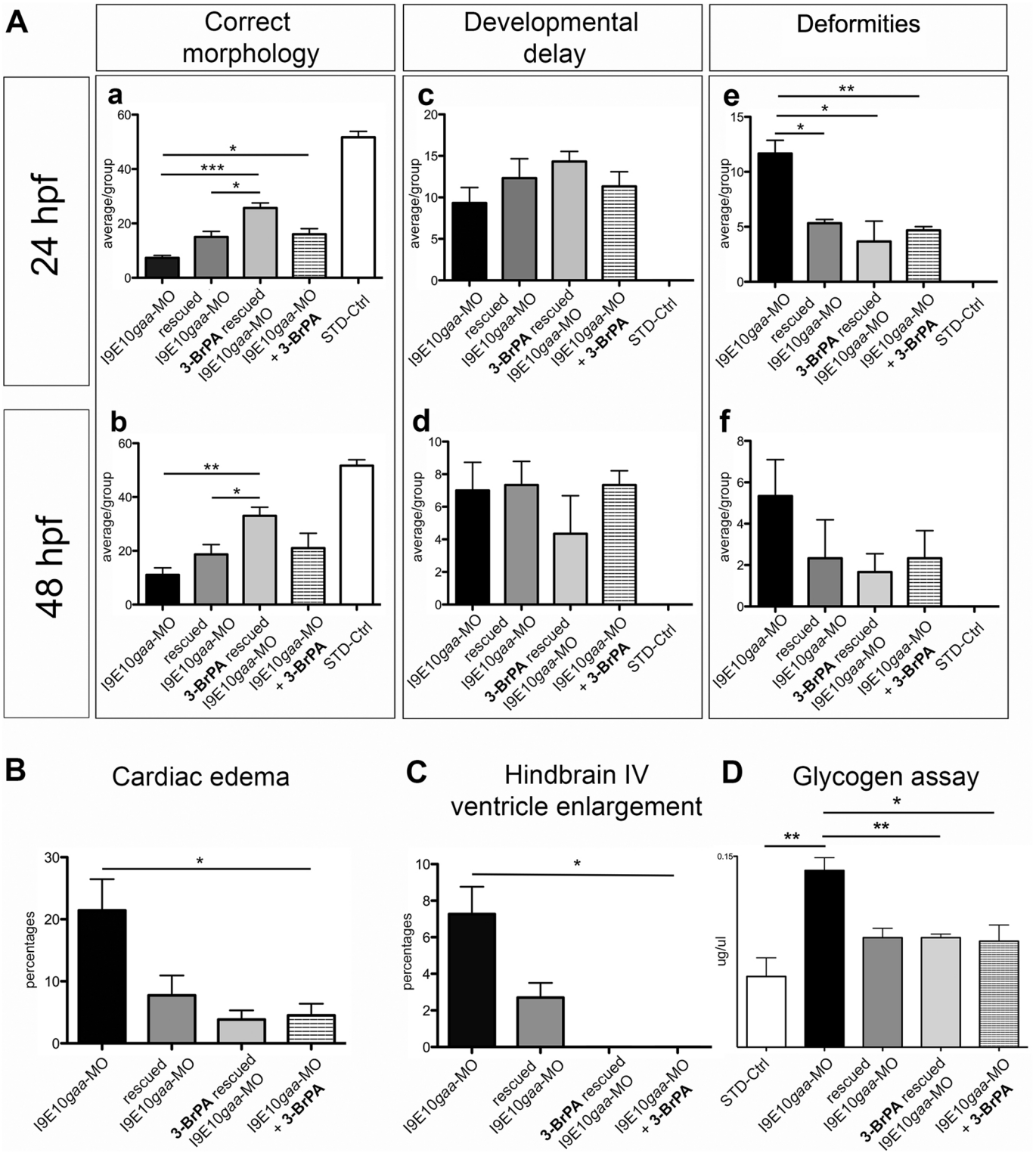
A
Correct morphology
Developmental delay
Deformities
24 hpf
48 hpf
a
b
c
d
e
f
average/group
l9E10gaa-MO
rescued l9E10gaa-MO
3-BrPA rescued l9E10gaa-MO
l9E10gaa-MO + 3-BrPA
STD-Ctrl
B
Cardiac edema
percentages
C
Hindbrain IV ventricle enlargement
D
Glycogen assay
ug/ul

Figure 6

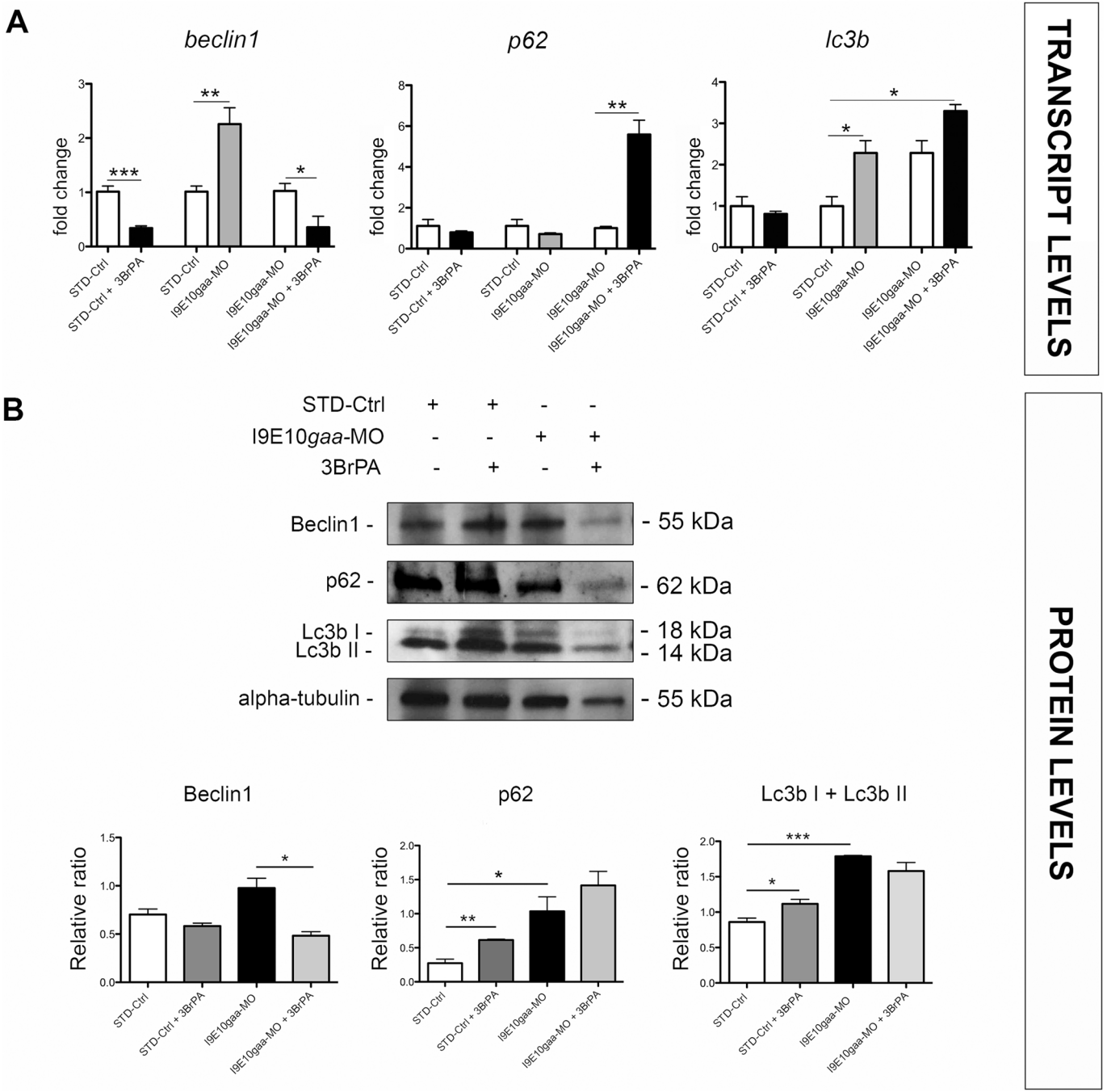
A
beclin1
p62
lc3b
fold change
STD-Ctrl
STD-Ctrl + 3BrPA
I9E10gaa-MO
I9E10gaa-MO + 3BrPA
TRANSCRIPT LEVELS
B
STD-Ctrl
I9E10gaa-MO
3BrPA
Beclin1 - 55 kDa
p62 - 62 kDa
Lc3b I - 18 kDa
Lc3b II - 14 kDa
alpha-tubulin - 55 kDa
Beclin1
p62
Lc3b I + Lc3b II
Relative ratio
PROTEIN LEVELS

Figure 7

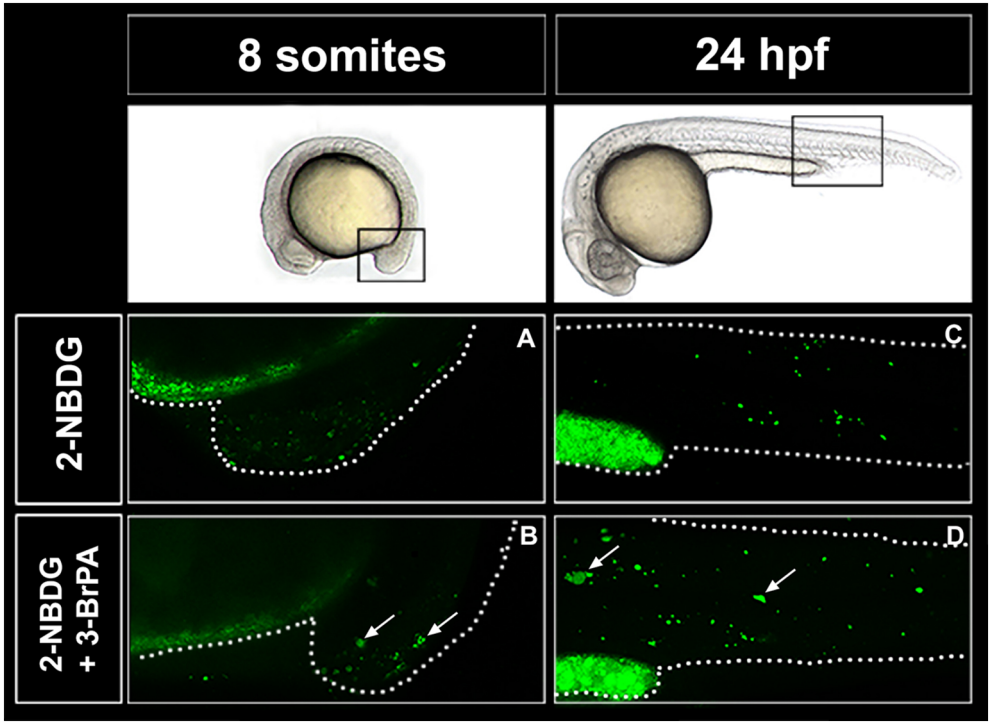

Figure 8

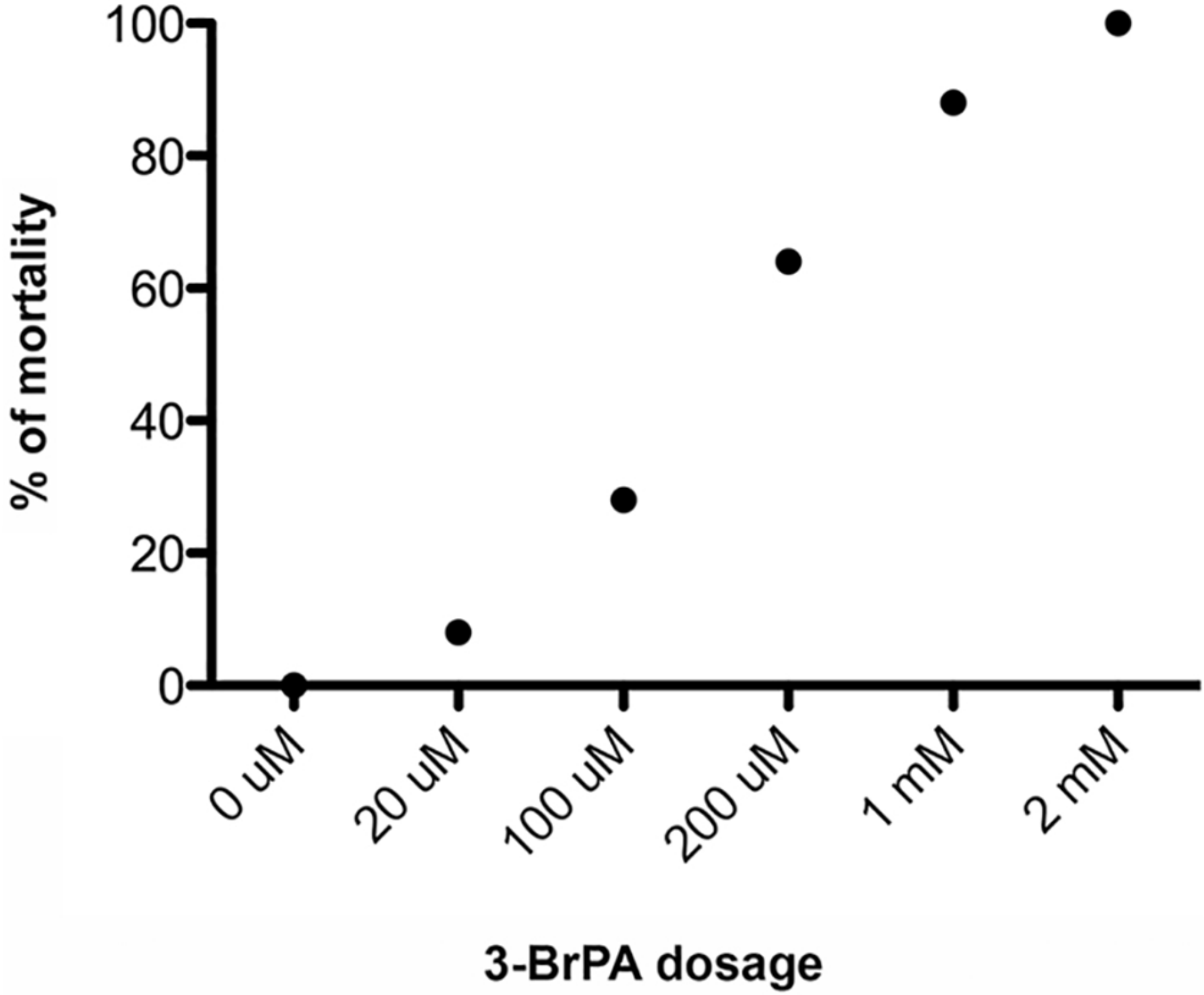
100
80
60
40
20
0
% of mortality
0 uM
20 uM
100 uM
200 uM
1 mM
2 mM
3-BrPA dosage

Figure 9

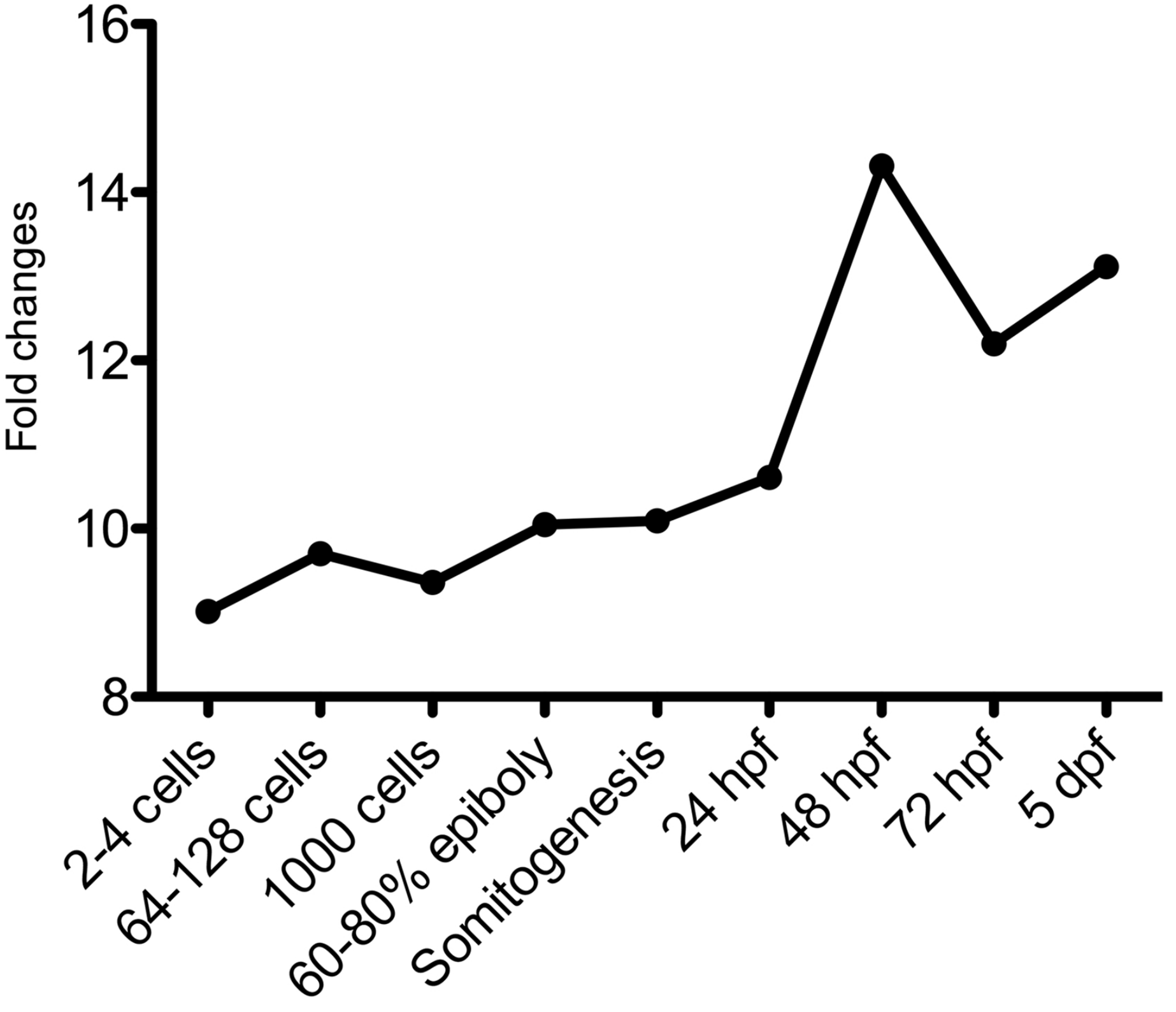
16
14
12
10
8
Fold changes
2-4 cells
64-128 cells
1000 cells
60-80% epiboly
Somitogenesis
24 hpf
48 hpf
72 hpf
5 dpf

Figure 10

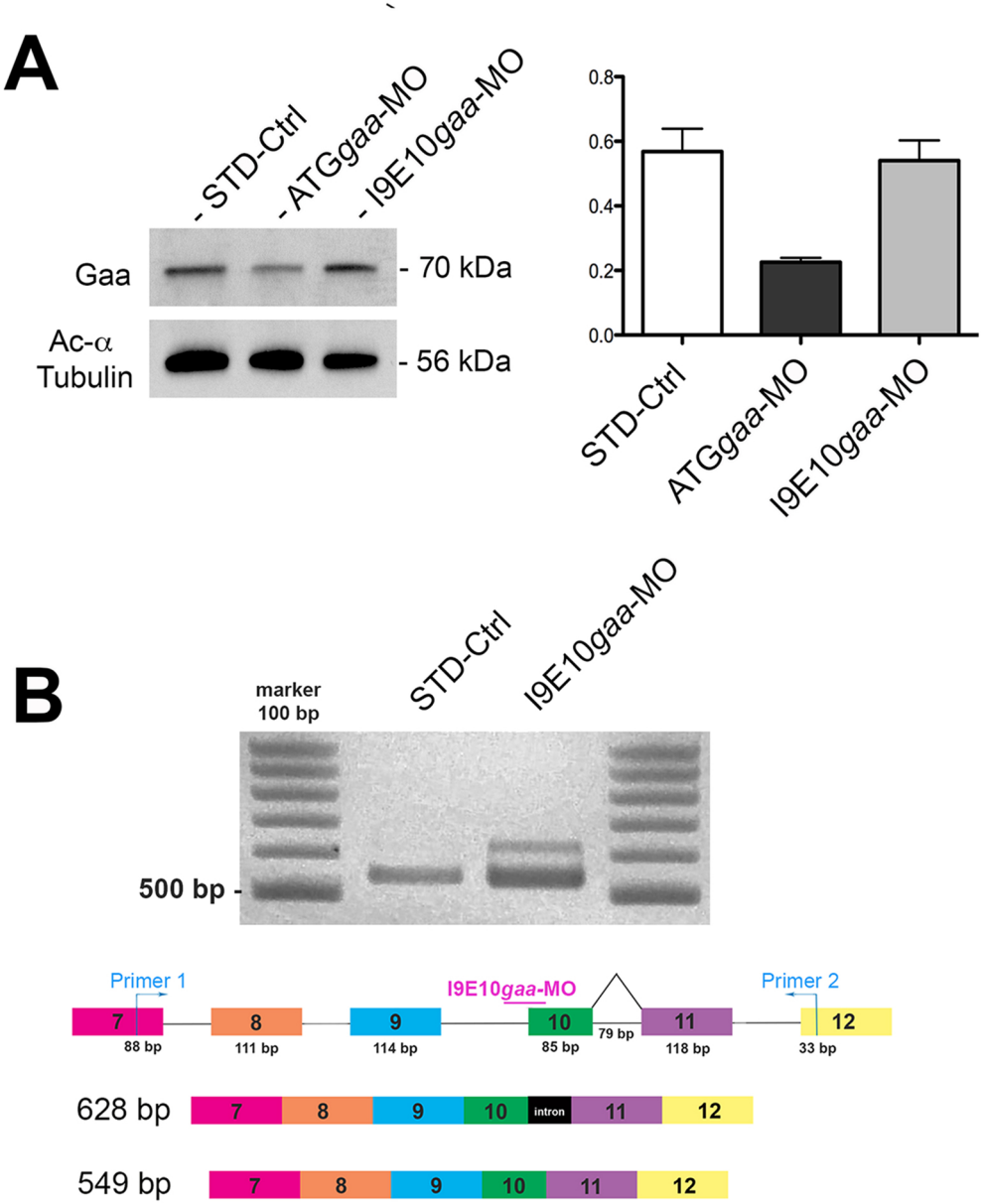
A
- STD-Ctrl
- ATGgaa-MO
- I9E10gaa-MO
Gaa
- 70 kDa
Ac-α Tubulin
- 56 kDa
0.8
0.6
0.4
0.2
0.0
STD-Ctrl
ATGgaa-MO
I9E10gaa-MO
B
marker 100 bp
STD-Ctrl
I9E10gaa-MO
500 bp -
Primer 1
I9E10gaa-MO
Primer 2
7
8
9
10
11
12
88 bp
111 bp
114 bp
85 bp
79 bp
118 bp
33 bp
628 bp
intron
549 bp

Figure 11

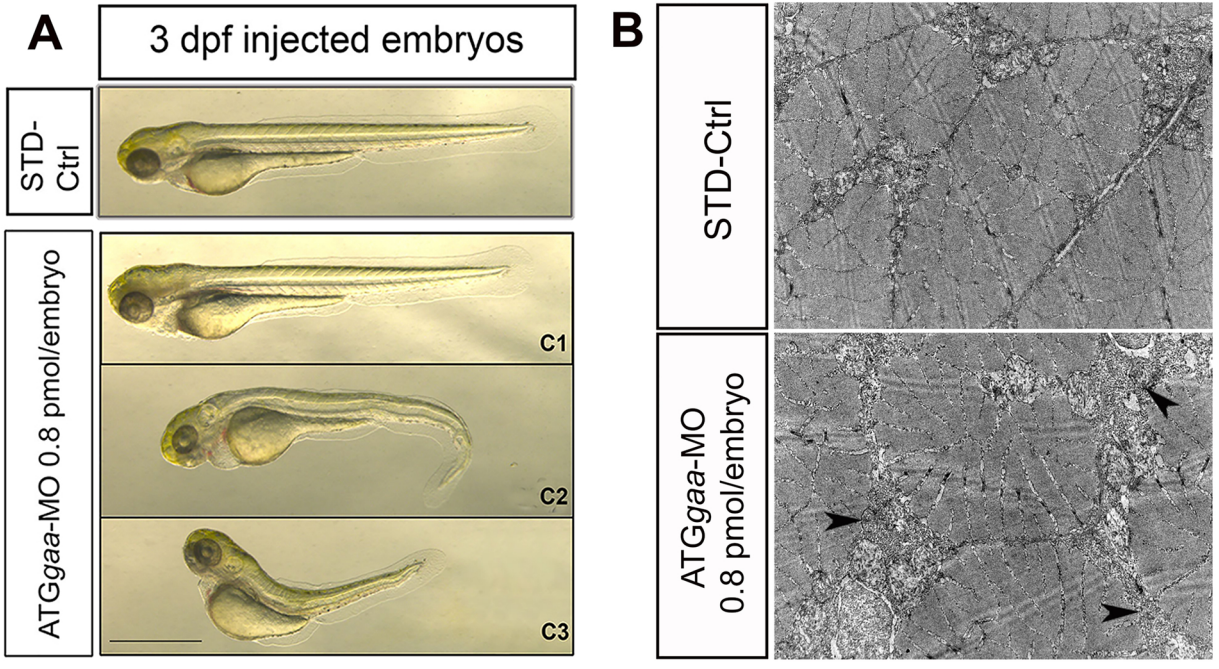
A
3 dpf injected embryos
STD-Ctrl
ATGgaa-MO 0.8 pmol/embryo
C1
C2
C3
B
STD-Ctrl
ATGgaa-MO
0.8 pmol/embryo

Figure 12

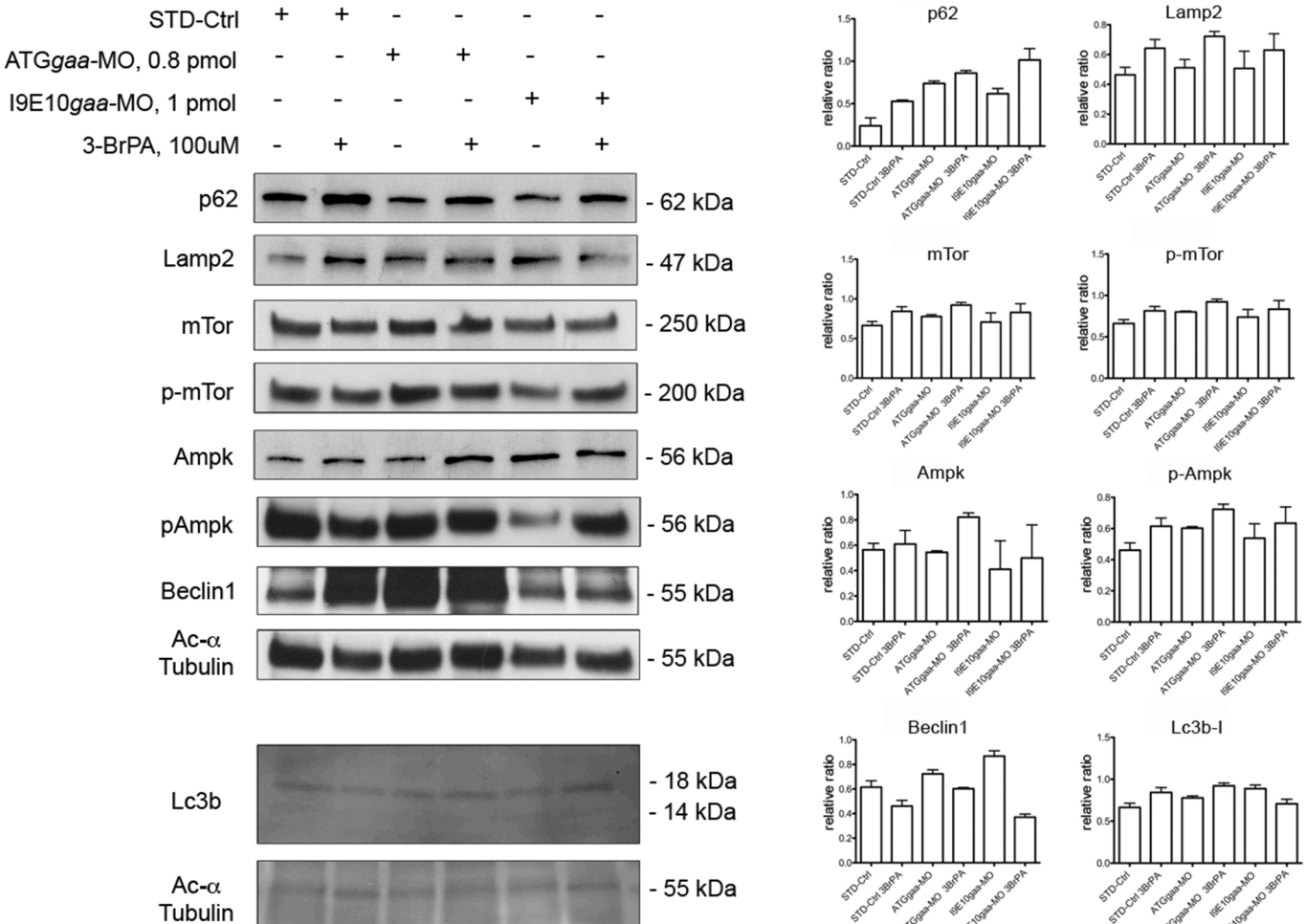
STD-Ctrl + + - - - -
ATGgaa-MO, 0.8 pmol - - + + - -
I9E10gaa-MO, 1 pmol - - - - + +
3-BrPA, 100uM - + - + - +
p62
- 62 kDa
Lamp2
- 47 kDa
mTor
- 250 kDa
p-mTor
- 200 kDa
Ampk
- 56 kDa
pAmpk
- 56 kDa
Beclin1
- 55 kDa
Ac-α Tubulin
- 55 kDa
Lc3b
- 18 kDa
- 14 kDa
Ac-α Tubulin
- 55 kDa
p62
Lamp2
mTor
p-mTor
Ampk
p-Ampk
Beclin1
Lc3b-I
relative ratio
STD-Ctrl
STD-Ctrl 3BrPA
ATGgaa-MO
ATGgaa-MO 3BrPA
I9E10gaa-MO
I9E10gaa-MO 3BrPA

Figure 13

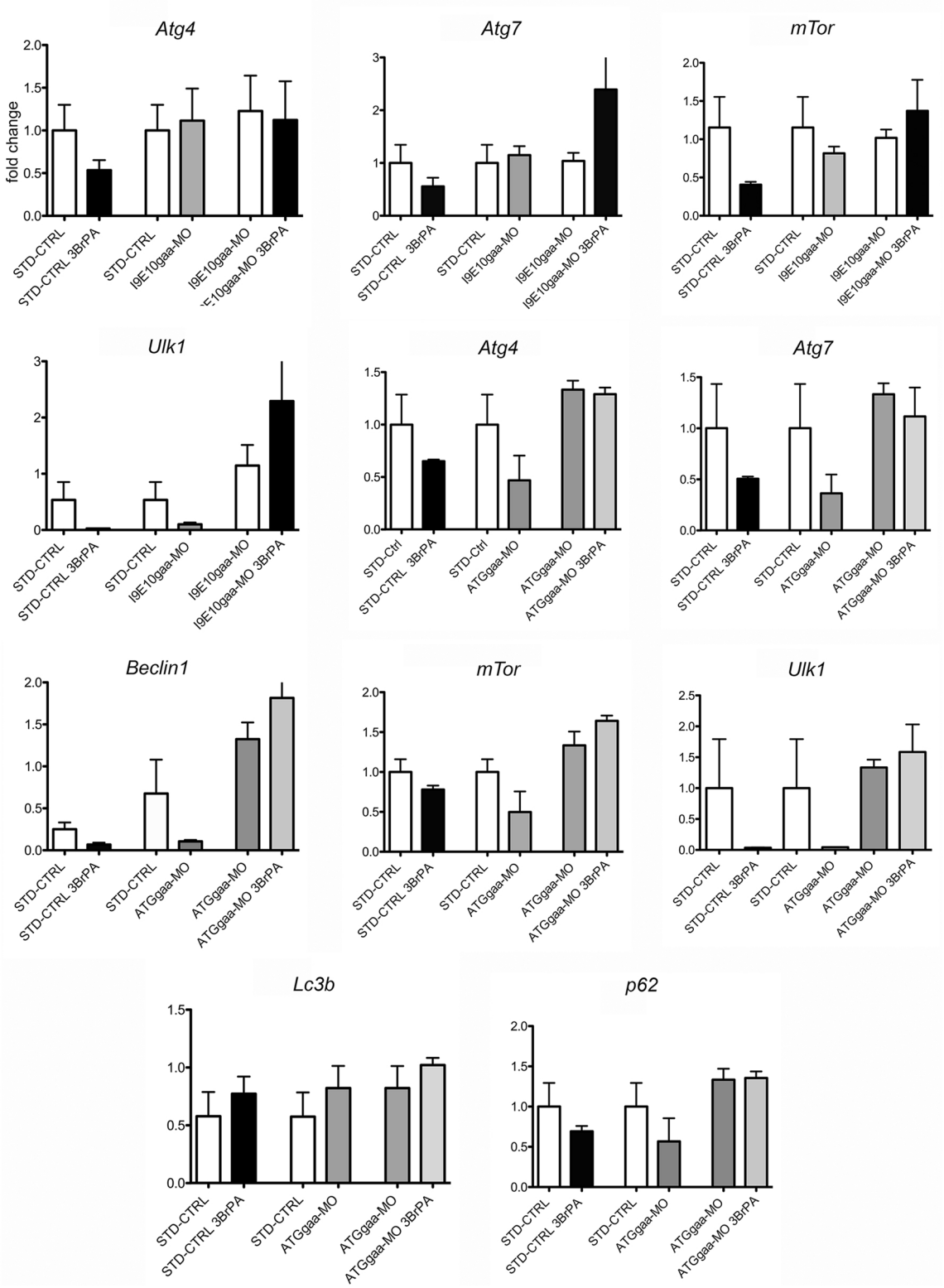
Transcript levels I9E10gaa-MO and ATGgaa-MO
Atg4
fold change
STD-CTRL
STD-CTRL 3BrPA
STD-CTRL
I9E10gaa-MO
I9E10gaa-MO
I9E10gaa-MO 3BrPA
Atg7
STD-CTRL
STD-CTRL 3BrPA
STD-CTRL
I9E10gaa-MO
I9E10gaa-MO
I9E10gaa-MO 3BrPA
mTor
STD-CTRL
STD-CTRL 3BrPA
STD-CTRL
I9E10gaa-MO
I9E10gaa-MO
I9E10gaa-MO 3BrPA
Ulk1
STD-CTRL
STD-CTRL 3BrPA
STD-CTRL
I9E10gaa-MO
I9E10gaa-MO
I9E10gaa-MO 3BrPA
Atg4
STD-Ctrl
STD-CTRL 3BrPA
STD-Ctrl
ATGgaa-MO
ATGgaa-MO
ATGgaa-MO 3BrPA
Atg7
STD-CTRL
STD-CTRL 3BrPA
STD-CTRL
ATGgaa-MO
ATGgaa-MO
ATGgaa-MO 3BrPA
Beclin1
STD-CTRL
STD-CTRL 3BrPA
STD-CTRL
ATGgaa-MO
ATGgaa-MO
ATGgaa-MO 3BrPA
mTor
STD-CTRL
STD-CTRL 3BrPA
STD-CTRL
ATGgaa-MO
ATGgaa-MO
ATGgaa-MO 3BrPA
Ulk1
STD-CTRL
STD-CTRL 3BrPA
STD-CTRL
ATGgaa-MO
ATGgaa-MO
ATGgaa-MO 3BrPA
Lc3b
STD-CTRL
STD-CTRL 3BrPA
STD-CTRL
ATGgaa-MO
ATGgaa-MO
ATGgaa-MO 3BrPA
p62
STD-CTRL
STD-CTRL 3BrPA
STD-CTRL
ATGgaa-MO
ATGgaa-MO
ATGgaa-MO 3BrPA

Figure 14

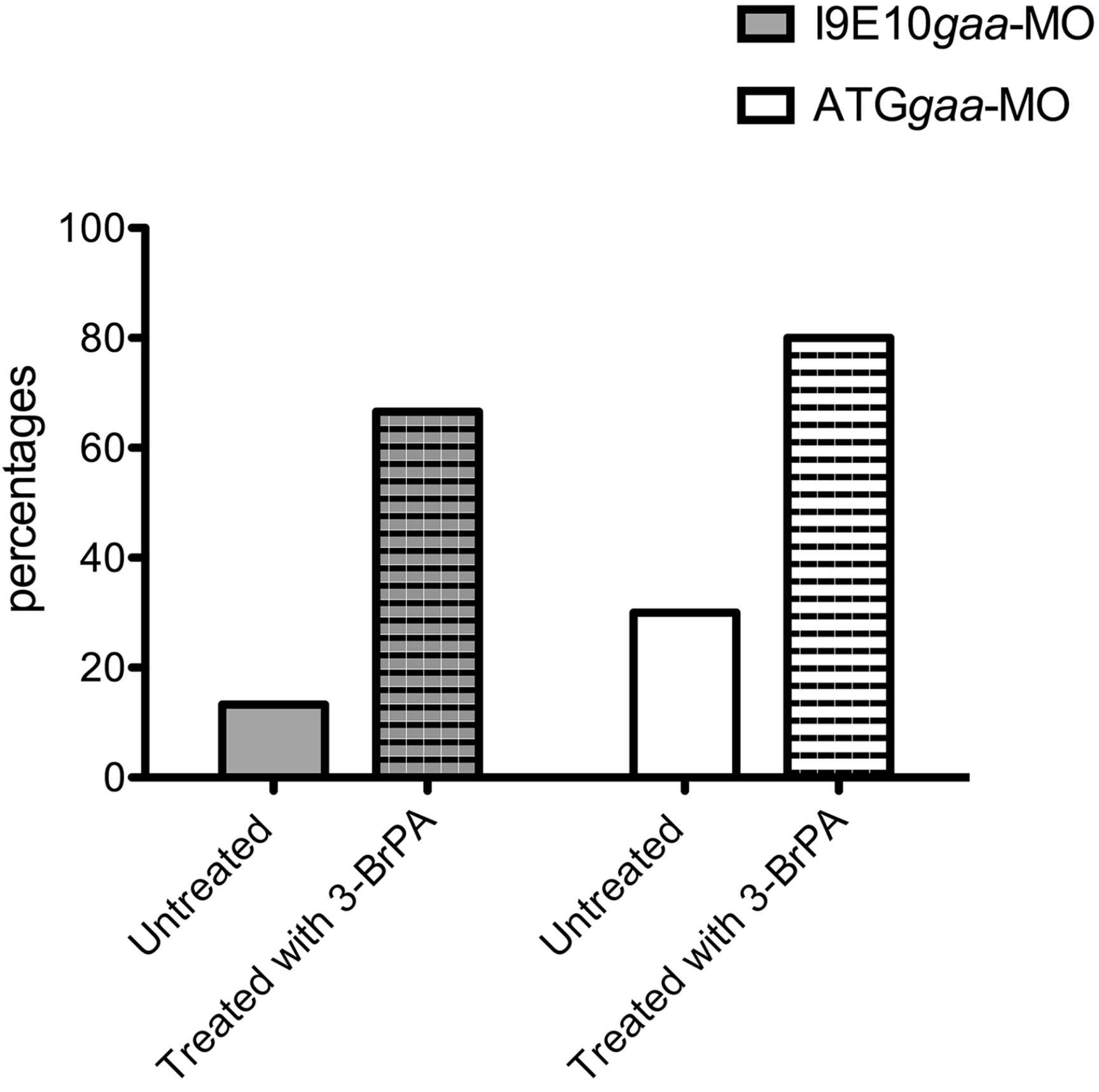
I9E10gaa-MO
ATGgaa-MO
100
80
60
40
20
0
percentages
Untreated
Treated with 3-BrPA
Untreated
Treated with 3-BrPA

Figure 15